Chaos ARTICLE pubs.aip.org/aip/cha

Detecting deterministic chaos in a high-complexity fire model

Cite as: Chaos 36, 043137 (2026); doi: 10.1063/5.0306306
Submitted: 9 October 2025 · Accepted: 4 April 2026 ·
Published Online: 30 April 2026

View Online Export Citation CrossMark

Jenna Sjunneson McDanold,[1,2,a] Alex Jonko,[1] Kara Yedinak,[3] Rod Linn,[1] Sophie Bonner,[1] Alexander Josephson,[1] and Nishant Malik[2]

AFFILIATIONS

[1] Los Alamos National Laboratory, Earth and Environmental Sciences, Los Alamos, New Mexico 87545, USA
[2] School of Mathematics and Statistics, Rochester Institute of Technology, Rochester, New York 14623, USA
[3] U.S. Forest Service, Building and Fire Sciences, Forest Products Laboratory, Madison, Wisconsin 53726, USA

[a] **Author to whom correspondence should be addressed:** jennasmcd@lanl.gov

ABSTRACT

Sensitivity to wind behaviors has been observed in marginal fire behavior in the field and using high-complexity fire models. Here we use the coupled atmospheric hydrodynamic-fire behavior model FIRETEC to simulate a marginal fire and develop 2028 one-dimensional time series from the temperature of the solid fuel, the convective heat transfer, the magnitude of the horizontal winds, and the vertical wind velocity on and around the leading edge of the fireline. We test each of these time series for chaotic signals using the Chaos 0-1 test that distinguishes between chaotic and non-chaotic time series. We analyze the spatial relationships with the leading edge by including series built from in front of and behind the leading edge of the fireline. We find that the length of the time step can cause a break in the determinism and, therefore, test the series for stochasticity using permutation entropy. We find the leading edge of the fireline to be highly chaotic and spatially correlated. We discuss some challenges in simplifying the time series for application with existing one-dimensional algorithms and discoveries that will lead to future work.

The complexity of fire dynamics makes understanding and predicting this phenomenon challenging. While the physics of fire behavior has been and continues to be studied extensively, examining fire using methods of nonlinear dynamics may offer new insights into whole-system dynamics. We use a hydrodynamic model of coupled atmosphere-fire behavior configured for marginal fire conditions to develop thousands of one-dimensional time series centered around the movement of the leading edge of the fireline. We test these series for chaotic or non-chaotic dynamics and stochastic or deterministic signals. We find that the leading edge of the fireline and locations within the fire are chaotic, whereas positions in front of the fireline tend to be more organized and non-chaotic. We also examine the role that the temporal gap between entries in the series has on the determinism of the simulation results. Since fire is a three-dimensional system relying heavily on dynamic atmospheric interactions between the fire activity and the surrounding air, a time step commensurate with these dynamics is necessary to capture local feedback and dependencies in only a single dimension. Our analysis is constrained by the reduction in dimension necessary for the use of the existing algorithms for detecting chaos in time series. We discuss our results in detail, along with the hypotheses for some of the unexpected dynamics we observe.

I. INTRODUCTION

There is a widespread misconception that chaotic systems are incomprehensible due to their complexity. In fact, chaotic systems possess inherent structures and characteristics that reveal repetitive patterns and deterministic behavior, even amidst apparent randomness. These systems are governed by mathematical rules, which, when understood, can lead to meaningful predictions within certain constraints. Wildland fire in some scenarios has been posed as possibly being a chaotic system as it can be sensitive to the details of surrounding conditions,[1,2] implying a "sensitivity to initial conditions." Yet, if all conditions are identical, it is reasonable to assume we would see the same fire behavior, implying a quality defined as "determinism." Thinking about wildland fire as a chaotic system is particularly interesting because it adds critical context to our expectations of fire predictability and framing for our fire modeling goals given that the precise details of initial and boundary conditions for wildland fire are seldom fully known. By mathematically defining fire behavior as chaotic, we seek to discover relationships between its system components and some underlying patterns that contribute to the apparent irregularity of the system.

Oxygen, heat, and fuel are the three components that influence fire dynamics.[3] However, the simplicity of this "fire triangle" can be misleading, as various aspects of the fire environment influence the feedback between these factors over a variety of temporal and spatial length scales. For example, the topography of the fuel bed influences the convection and radiative heat transfer.[4–6] Differences in litter accumulation or treatments in a given area can change the surface and ladder fuels and lead a lower-intensity fire to develop into a high-intensity crown fire.[7–9] The dynamic fire-atmosphere interactions can lead to unique phenomena like fire whirls and counter-rotating vortices in and around the flames.[10–12] These types of heterogeneous and dynamic feedback influences on the basic controlling factors of wildland fire exemplify chaotic behavior.

To further our understanding of fire dynamics, we need to examine the macroscale behavior. Collecting sufficiently detailed and comprehensive data in the field is challenging given the complex multi-faceted, dynamic, and multi-scale interactions occurring in the fire environment. However, we can use models that represent feedback between basic physical processes to simulate emergent fire behavior to provide some of this information. In particular, numerical models offer us the ability to collect temporally evolving and spatially explicit data associated with numerous dynamic aspects of the fire environment and fire activity, allowing unique opportunities to study the feedback between the fire and its surroundings that are currently very challenging with observations. It is important to acknowledge the limitations of numerical models as they do not represent the complete set of physical and chemical processes at all relevant scales. Even though models may lack some of the physical processes, the fact that modern physics-based wildfire models such as the Wildland Fire Dynamics Simulator[13] and FIRETEC[14] focus on representing basic physical processes in order to simulate aggregated and emergent fire behavior including feedback between fire and the surrounding atmosphere make them a valuable tool for studying fire dynamics and a great complement to field and laboratory observations.

There is some debate on the formal definition of chaos, but it is generally accepted to include at least three features: sensitive dependence on initial conditions, determinism, and aperiodic long-term behavior.[15–20] Sensitive dependence on initial conditions implies that a very slight change in an initial condition can result in vastly different outcomes. Deterministic behavior implies that any noisiness within the outputs are a result of the nonlinearity of the system, not any stochastic components. Specifically, a unique input to a deterministic system will always result in a corresponding unique output for any number of trials, whereas a stochastic system may produce a variety of outputs for any given input. Aperiodic long-term behavior is characterized by trajectories that do not converge into any kind of periodic behavior (i.e., limit cycles, stable fixed points, or quasiperiodic orbits). This is a secondary result of the combination of determinism and sensitive dependence on initial conditions; since no trajectory ends up exactly where any previous trajectory has been (unique inputs lead to unique outputs), no matter how close those trajectories are, there will be long-term divergence between them (sensitivity to initial conditions).

Chaos theory is a cornerstone of modeling complex systems in many genres of science[20,21] including astrophysics,[22–24] geophysical systems,[25–29] biological and medical sciences,[30,31] and has even been used for the social sciences[32] and building construction.[33] The sciences are particularly suited for chaos theory due to their high level of complexity and interdependent processes. Measurement of these inter-relationships and the effect each process has on the whole system can be achieved through studying the nonlinear nature of the dynamics.[34] Specifically, chaos theory and fractal analysis have been used in seismology to model aftershocks and earthquake probability[27,29] and has led to the development of wavelet transforms for earthquake characterization.[29] The fields of gravity and magnetism have used chaos theory to find causative sources and characterize their qualities for future prediction.[26] Chaos theory has also been used to examine a variety of qualities of fluid flow, including runoff and river flow,[25] chaotic advection in oceanic flow,[28] and weather prediction,[15] and has found relationships between flow systems on a global scale.[35] Chaos has been detected in tracking planetary orbits and relationships between planetary bodies.[22–24] In general, chaos theory allows us to assess prediction possibility, evaluate model validity,[36] identify key processes within the phenomenon,[34] and determine the degrees of freedom in a process to assist in developing simple systems of equations for representing these phenomena.[37]

As with these other fields of study, studying wildland fire behavior using chaos theory may help us interpret and understand this system so as to develop more effective predictive models and identify the key processes underlying unexpected behavior. The identification of chaotic phenomena in large-scale fire models such as FIRETEC highlights the inherent complexities involved in predicting fire dynamics over extended periods. These chaotic behaviors can lead to significant variabilities in fire spread and intensity, making it difficult to achieve accurate long-term forecasts. Furthermore, these observations offer valuable insights into the development of reduced-order models of fire dynamics. To enhance their effectiveness, it is essential that these models incorporate nonlinear characteristics that reflect the chaotic nature of fire behavior. By doing so, researchers can improve the fidelity of simulations, providing a more nuanced understanding of how various factors such as fuel sources, meteorological conditions, and terrain interact and influence the progression of wildfires. Ultimately, this could lead to more robust predictive tools, better informing fire management strategies and improving response efforts in real-world scenarios.

Previous work has identified some chaotic qualities in fire behavior already. Through field collected data from nine burns on different plots, Clements *et al.*[1] demonstrated sensitivity to initial conditions when they observed that low-intensity fires are sensitive to shifts in near-surface wind dynamics. Then Linn *et al.*[38] used one of those experimental burns to inform a FIRETEC simulation to further illustrate that small changes in the windfield can have a broad effect on fire behavior, and Jonko *et al.*[2] used an ensemble approach in which they compared 45 FIRETEC simulations with identical conditions except for small perturbations in the ambient wind field. These studies clearly indicate that macroscopic fire behavior is sensitive to small perturbations in wind conditions. This sensitivity is a hallmark feature of chaos and nonlinear dynamics.

So far, there have been several studies done on the nonlinear dynamics of fire behavior. Turcotte *et al.*[39] found self-organized criticality in the frequency of forest fires relating to the area burned, promoting the concept of scale-invariance in fire occurrence. Self-organization is a feature of some dynamical systems in which the system parameters spontaneously adjust such that pattern formation occurs. Self-organized criticality implies that these parameters automatically adjust to guide the system toward a phase transition when close to the critical point attractor, as defined in Bak *et al.*[40] Scale-invariant means that the spatial and temporal macroscopic behaviors do not change when control parameters are scaled by a constant factor. Similarly, Ricotta *et al.* also examined self-organizational trends in wildfire occurrence in Liguria, showing that the ignition mechanism may have the most impactful effect on how it organizes.[41]

The most recent example of chaos theory applied to fire behavior presents a discrete set of equations developed from a reaction-diffusion equation, similar to the derivation of the Lorenz equations for wind dynamics.[15,42] The goal of that study was to predict the transition from stable to unstable behavior in a wildfire for risk assessment and Decision Support Systems. Mampel *et al.*[42] assumed that fire is chaotic due to the influence of the winds which are known to be chaotic. To support this assumption and show that fire behavior is mathematically chaotic, we use a hydrodynamic model of coupled atmosphere-fire behavior called FIRETEC, configured for marginal fire conditions. We develop 2028 one-dimensional time series related to the movement of the leading edge of the fireline and employ nonlinear time series analysis to detect the presence of chaos in model-derived fire behavior.[43,44]

Algorithms designed for chaotic signal detection are typically developed for univariate time series, and it is, therefore, necessary to reduce the dimensionality of multidimensional data prior to applying these methods. This reduction, however, can alter the structures and patterns in the data and introduce unexpected artifacts. For instance, data generated by a simulation such as FIRETEC are discretized in both space and time, while the model itself operates across three spatial dimensions in order to capture and resolve the complex wind dynamics of the environment. Distilling this multidimensional information into a single univariate series may alter the perceived structure of the data in non-trivial ways, such as introducing apparent stochasticity or obscuring pertinent features of the underlying chaotic attractor. While such limitations cannot be entirely avoided, we have taken care to mitigate their effects by increasing the temporal resolution and rigorously testing the reduced data for stochastic properties. Our methodological choices regarding dimensionality reduction and their potential implications for our results are discussed in detail in Sec. III.

II. DATA

Over the last 60 years, wildland fire growth modeling has evolved markedly. Most notable is the transition from purely empirical models[45–50] to a more nuanced approach that incorporates physical processes, including hydrodynamics surrounding wildland fires in the larger complex environment.[13,14,51,52] FIRETEC is one such hydrodynamic model that has been utilized in numerous studies, including those examining fire propagation,[53] fire effects,[14,54] and the impact of fuel treatments.[55] We choose this model because it conserves mass, momentum, and energy, and features spatial and temporal resolutions that are appropriate for analysis of the feedback between fire and its surroundings.

To determine if chaotic signals are present in fire behavior, we want to limit the different types of fires we study to avoid mixed dynamics. We choose to study only the "heading" fire behavior that occurs at the traveling front of the fire driven by local winds, ignoring the flanking (lateral) and backing (opposed flow) fire growth.[56] Our FIRETEC simulations are designed to target "marginal" scenarios in which fire growth is at the tipping point of extinguishment and sustained combustion. We choose these conditions because the transition between these states tends to be highly sensitive to atmospheric and surface conditions. The sensitivity to wind dynamics observed in low-intensity fire field experiments[1] and previous FIRETEC simulations[2,38] inspires the possibility that a transition into chaos is possible in these types of fires.

A. FIRETEC

FIRETEC is an Eulerian Computational Fluid Dynamics model simulating the spatiotemporal behavior of fire using Cartesian (x, y, z) spatial coordinates. In order to simplify the fire scenario and increase the robustness of our analysis, we use a simulation that represents a grass fire that is propagating in line with the primary wind direction (see Fig. 1). We use horizontal resolution of $2 \times 2\,\text{m}^2$ for each cell. We have 41 vertical cells (z direction) employing a cubicly stretched grid ranging from $\approx$1.5 m tall near the surface to $\approx$40 m tall near the top of the domain, resulting in a total height of 615 m.[51] We create a fire scenario where every location (x-coordinate) along the fireline is exposed to the same macroscale fire environment as every other location and, thus, they can all be taken as equal members of an ensemble. In order to achieve sufficiently long time series for our analysis, we use a 1200 cell long domain in the direction of the primary wind direction (along the y-axis). Fuels (vegetation) are resolved in three dimensions at the model's grid resolution using a volumetric porous media with mass momentum and energy exchange. The gas phase is characterized by fuel related parameters such as moisture, surface area per unit volume, fuel height, and density. We limit our fuel to homogeneous grass to reduce the number of variables that could affect the fire behavior and change our results. The grass fuel is 0.3 m tall with a fuel density of $0.3\,\text{kg/m}^2$ and 15% fuel moisture. FIRETEC represents fuels that are shorter than the first vertical grid cell by distributing their bulk properties (e.g., mass, volume, and drag elements) uniformly within that cell. The model then incorporates fuel height in its calculation of wind drag, so shorter fuels impose proportionally less drag on the flow. The domain setup for five separate time steps can be seen in Fig. 1.

In order to establish the turbulent wind conditions, we represent the turbulence developed over a very long upwind fetch using a $400 \times 2400\,\text{m}^2$ domain. We simulate a wind field where the primary wind direction flows along the y-axis (2400 m long) of the domain with an average speed of 6 m/s. Initially, the winds in this simulation

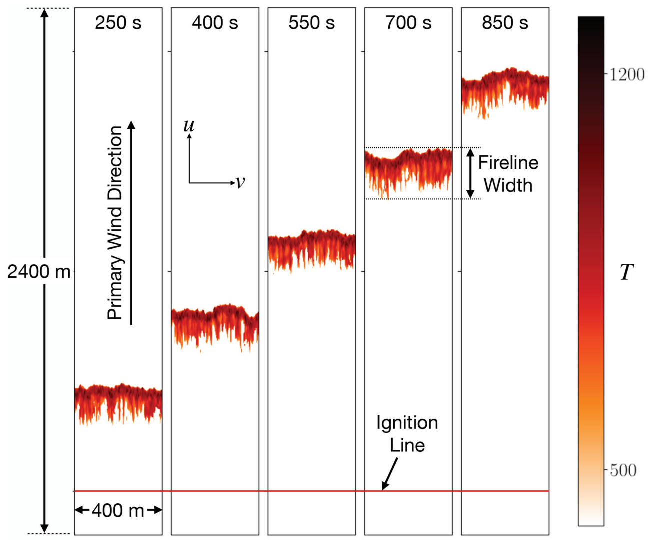

FIG. 1. Diagram of FIRETEC setup showing five time steps in the simulation visualizing the temperature of the solid, $T \geq 500$ K. Moving from left to right, the visuals move forward in time from 250 s through 850 s in 150 s increments. Diagram shows the length and width of the domain along with the horizontal wind directions (u and v), the primary wind direction (u), the measurement of the fireline width, and the location of the ignition line.

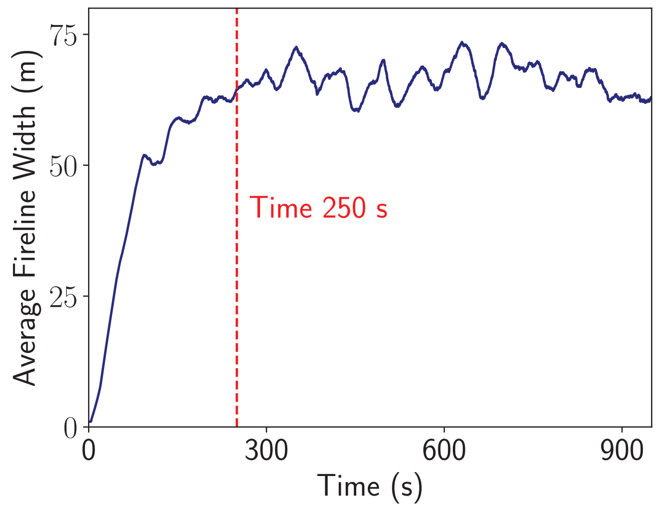

FIG. 2. Average fireline widths for each time step; vertical line at 250 s shows the starting point for each time series developed. Note that at 250 s, we have reached a level average state after the initial ramping of the fire behavior due to ignition.

are uniform across the domain. Turbulence is induced by randomly placing blocks of vegetation in the lowest five layers of the domain ($1 \leq z \leq 5$). These blocks, which are similar in concept to the baffles used to accelerate turbulence development in wind tunnel experiments, perturb the flow field, causing variation in the winds and developing turbulence. We use this wind field to inform the fire simulation as initial and boundary conditions and to interact with the fire-induced changes in turbulent flow.

During the fire, cyclic boundary conditions on the sides essentially make the domain laterally infinite,[57,58] allowing flow to pass through the boundary on one side, and back into the domain on the other side. This permits us to consider each x-coordinate as a separate "fire event" for our time series and virtually eliminates any lateral edge effects for the simulation that may interfere with the study. We place an ignition line 100 cells away from the upstream domain boundary. This distance ensures minimal boundary effects. The ignition line has a thickness of 2 cells or 4 m. We "ignite" each $x \in X$ along this transect by removing all fuel moisture and linearly increasing the temperature of the solid, T, to 1000 K over the first 3.5 s of the simulation.[51]

Since this ignition procedure is non-physical, we want to exclude its effects from the analysis. Thus, we discard the initial several minutes of the simulation, during which these impacts are felt. We begin analysis once the fireline width has reached a pseudo-steady state. The fireline width is defined as the distance between the cells closest to and farthest from the ignition that have reached an average temperature $T \geq 500$ K, as is illustrated in Fig. 1. Figure 2 shows the average fireline width for each time step of our simulation with a vertical line at 250 s, after which point the average fireline width has stabilized. The end of the simulation is defined to be before the fireline reaches the end of the domain. We record simulation data from 250 s through 950 s after ignition, creating 7001 records per series with time difference of 0.1 s between records. For the rest of this paper, we will refer to this time difference as a "time step," but we want to be clear that this output data "time step" is not the same as the computational time step used for some of the processes in FIRETEC, which was 0.001 s. This is the smallest practical time step we were able to accommodate while still producing reasonably accurate data. This limitation is largely governed by computational cost. Generally, FIRETEC will create 0.6 simulated seconds per hour for this particular domain configuration, while recording output for every time step. To decrease the time step in this case would require significantly more time for the model to run than is feasible.

The advantage of using FIRETEC for this analysis is the large amount of information produced from the simulation. We use two fire variables: the convective heat transfer (Q) and the temperature of the solid fuel (T); and two wind variables: the horizontal wind magnitude ($U = \sqrt{u^2 + v^2}$) and the vertical wind velocity (w), each defined in Table I. Each of these variables is computed as cell-wide averages for each time step per cell in the $200 \times 1200 \times 41$ cell computational grid. The convective heat transfer, Q, is the thermal energy transferred from the gas to the solid fuel in a cell due to the movement of gas over the solid surface and has units W/m^3. T is measured in Kelvin (K) and is defined as the temperature of the combination of the grass and associated fuel moisture (the "solid"). The wind variables both have units of m/s. For a detailed description of the governing equations in FIRETEC for the variables we choose to study, see Appendix A.

It must be explicitly acknowledged that FIRETEC is a large, complex computational model whose inherent configurability constitutes a meaningful limitation that warrants careful consideration

TABLE I. Table showing each variable from FIRETEC used in our analysis. We use a cell defined as (x, y) with $x \in X = \{1, 2, 3, \ldots, 200\}$ and $y \in Y = \{1, 2, 3, \ldots, 1200\}$.

Variable	Description	Units
Q	Convective heat transfer: the transfer of thermal energy from the gas to the solid within a given cell.	W/m^3
T	Temperature of the combination of the fuel and the water within the grass within a given cell.	K
U	Magnitude of the horizontal wind trajectories, $u_{x,y}$ and $v_{x,y}$ for a given cell; $\sqrt{u_{x,y}^2 + v_{x,y}^2}$.	m/s
w	Velocity of the vertical wind trajectory for a given cell.	m/s

when interpreting the findings presented in this study. Given that the model encompasses a broad array of adjustable parameters and toggleable capabilities, alternative configurations could plausibly yield divergent outcomes, and no single configuration can be presumed to produce universally generalizable results. The authors are fully cognizant of this constraint and underscore that a truly exhaustive, configuration-spanning analysis—one capable of substantiating claims of broad generalizability—would demand a level of computational resources that renders it prohibitive within the practical boundaries of the present investigation.

B. Time series

FIRETEC output is Eulerian (values recorded at fixed locations associated with each computational cell per time step). To determine the presence of chaotic behavior in the changes for each variable through time and space, we choose a Lagrangian style time series to track the evolution of quantities at specific positions relative to the moving fire front (not relative to the fixed computational grid). To convert the Eulerian data to a Lagrangian format, we define a moving reference frame associated with the traveling fire front. We track the movement of the fireline through time for specific positions in the computational grid (each x-coordinate). The fireline, referred to hereafter as $Y_s(x)$, is defined as the series of spatial streamwise positions (y-coordinates) farthest from the ignition line that achieve a temperature of the solid $T \geq 500$ K for each time step $s \in S = \{250.0, 250.1, \ldots, 950.0\}$. Figure 3 shows a snapshot of 280 s into the simulation. Note the broad area with active combustion ($T \geq 500$ K) in black. The white line at the top of the black area depicts the leading edge of the fire ($Y_s(x)$) as it progresses upward.

Using the fireline, $Y_s(x)$, we develop a variety of time series that investigate the fire behavior from several perspectives. Table II gives a list of the time series developed from the x-coordinates in the domain. We use coordinates that are perpendicular to and inline with the direction of movement of the fireline, referred to as the "primary wind direction" in Fig. 1. The three sets of series described in Table II are created using every 5th cell from $5 \leq x \leq 195$ and each of the four variables is described in Table I and in Appendix A. By choosing every five cells, we limit the possibility of redundancy in our time series due to overlap.

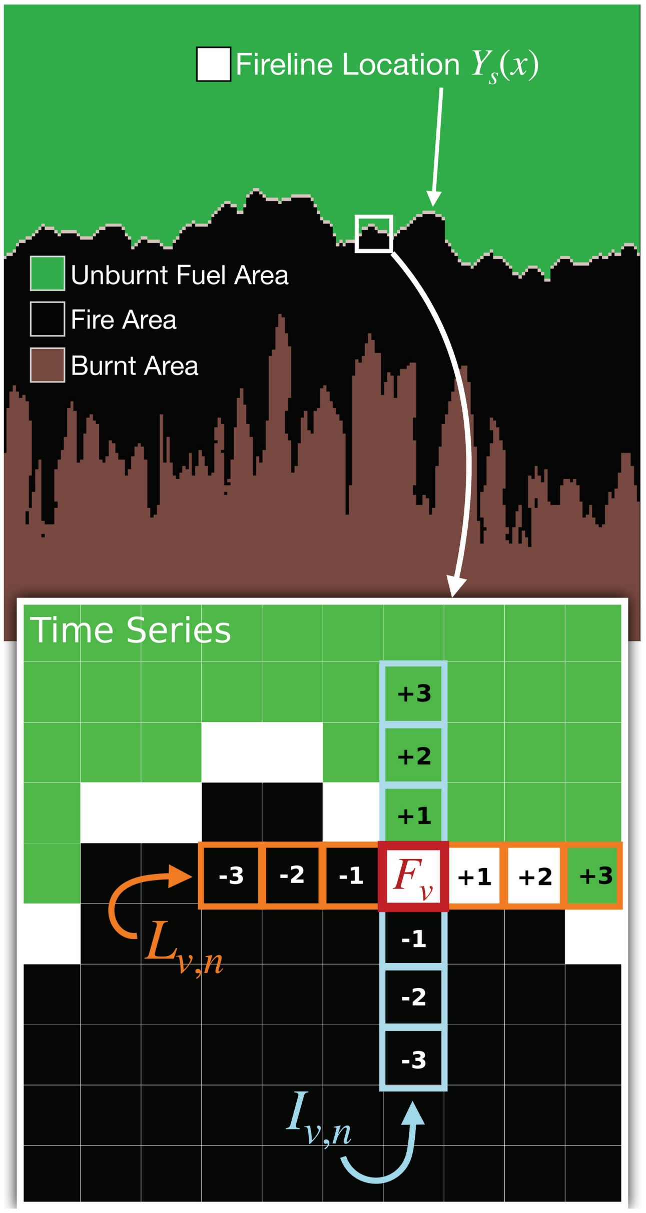

FIG. 3. Top down visualization of the time step related to 280 s from the FIRETEC simulation. The fireline location is defined as $Y_s(x)$ for the y-coordinate at location $x \in X = \{5, 10, 15, \ldots, 195\}$ at time $s \in S = \{250.0, 250.1, \ldots, 950.0\}$. $F_v(x)$ is the value of the variable $v \in V = \{Q, T, U, w\}$ at location $Y_s(x)$. The fireline location is in off-white, the unburnt fuel area is in green, the burnt area is in brown, and the locations that are actively on fire are in black. The small white box is blown up below to show the time series locations as offsets from the fireline.

For the equations that follow, we define these sets,

$$V = \{Q, T, U, w\}, \tag{1}$$

TABLE II. Table showing the various time series types we developed for this study that use each x-coordinate as a separate fire event. v represents the variable for the time series, n shows the offset from $Y_s(x)$, for all time steps s. See Eqs. (5) and (6).

Name	Description
$F_v(x)$	Values of each variable $v \in V$ for the fireline locations
$I_{v,n}(x)$	Values of each variable for cells in front and behind in line with $F_v(x)$
$L_{v,n}(x)$	Values of each variable for the fireline locations and lateral cells to the left and right, perpendicular to $F_v(x)$

which contains the matrices of variables that are produced by the simulation in the Eulerian grid and used to develop each of the Lagrangian series. Each of these variable matrices is 200×1200 cells, recorded from the FIRETEC simulation for each time step in the bottom vertical layer ($z = 1$). Then,

$$X = \{5, 10, 15, \ldots, 195\}, \tag{2}$$

defines the 39 x-coordinates used in this analysis. Likewise, the spatial offset coordinates for each time series N are defined such that

$$N = \{-3, -2, -1, 1, 2, 3\}. \tag{3}$$

The fireline, $Y_s(x)$, is defined as the y-coordinate for the fireline at time step s for a particular x-coordinate, such that $T(x) \geq 500$ K.

The base set of time series are built from the values of each variable at the fireline (in the Lagrangian frame moving with fire front), $(x, Y_s(x))$,

$$F_v(x) = \{v(x, Y_s(x))\}_{s\in S}. \tag{4}$$

We include a modified version of F_v defined as $\hat{F}_v$ in which we only consider every other time step in S, such that $S^* = \{250.0, 250.2, \ldots, 950.0\}$ and $\hat{F}_v(x) = \{v(x, Y_s(x))\}_{s\in S^*}$ for sensitivity testing purposes only, not to be included in the final test results.

The first set of series, $I_{v,n}(x)$, tracks each variable for the three coordinates with the same x position as the movement of $F_v(x)$, in front and behind $F_v(x)$ $\forall n \in N$,

$$I_{v,n}(x) = \{v(x, Y_s(x) + n)\}_{s\in S}. \tag{5}$$

The second set of series, $L_{v,n}(x)$ shows the value at corresponding lateral coordinates (same y position) to the left or right of each specific $F_v(x)$ for all $v \in V$ and $n \in N$,

$$L_{v,n}(x) = \{v(x + n, Y_s(x))\}_{s\in S}. \tag{6}$$

Note that each $v \in V$, $n \in N$, and $x \in X$ produces different series for each of these types, resulting in a total of 2028 different time series (507 per variable) used in this study. The above equations are visualized in Fig. 3. See Appendix A for more information on the governing equations used in FIRETEC.

III. METHODS

We quantify chaotic behavior in a wildland fire model by applying ergodic theory and Fourier Analysis, through the use of the Chaos 0-1 test (C01), developed in 2004 by Gottwald and Melbourne.[59] We assess the effect of the dimensional reduction by testing for stochasticity in our time series design using a model developed in 2021 by Boaretto *et al.*,[60] that calculates Permutation Entropy (PE) and compares it to known stochastic systems. Both of these methods are described in detail in the publications cited above and we give a general description of the concepts behind them below.

There are a variety of methods for detecting the presence of deterministic chaos in a time series. The most well-known include estimating the maximal Lyapunov exponent, for which there exist several algorithms,[20,61–67] and calculating fractal dimensions.[20,68] The process for calculating Lyapunov exponents measures the sensitivity to initial conditions by finding the rate of divergence between two trajectories that begin infinitesimally close together. The Lyapunov exponent is then defined as the exponential rate of divergence between these two points: a positive Lyapunov exponent indicating divergence and, therefore, chaos while a negative Lyapunov exponent indicating convergence and representing non-chaotic dynamics. Most often, the techniques used in calculating Lyapunov exponents and fractal dimensions require determining two parameters: the embedding dimension, the minimum dimension needed to reconstruct a topologically equivalent attractor to the attractor in the underlying data, and a time delay that removes any temporal correlations in the time series to avoid oversampling of the data which could suppress any chaotic signals. These parameters form the basis for phase-space reconstruction of the dynamical system underlying the time series. If we collect every possible state of a given dynamical system, we can define the "phase space" for that system, and using that space, we can track how the system behaves through time by following how the system moves through that phase space. Lyapunov exponents and fractal dimensions can be highly sensitive to the choices of these parameters and accurately redefining the phase space. Reliable evaluation of the values for these parameters from data can be extremely challenging for shorter time series, especially in the presence of noise.[62,63,65] Complicating things further, with a short time series, a time delay embedding can reduce the length of the series even further which increases the potential for lack of convergence in the method. On the other hand, without the embedding, we risk oversampling the data that flattens out the dynamics and can lead to false results.

The FIRETEC configuration employed in this study has been explicitly parameterized to suppress all stochastic processes within the model. However, it is argued that residual stochasticity may nonetheless manifest in the output time series as an artifact of the dimensional reduction procedure applied during preprocessing, as well as the constraints imposed on the inter-point spacing of the series. This emergent stochasticity, if present, poses a nontrivial methodological concern, as the C01 test is agnostic to the deterministic or stochastic nature of the underlying process and is, therefore, susceptible to yielding false positives when applied to stochastic time series. Consequently, it is deemed necessary to rigorously assess the stochastic character of the resultant output prior to drawing conclusions from the C01 statistic. A detailed discussion of the theoretical basis for this methodological decision, along with the corresponding diagnostic framework, is deferred to Sec. III B.

We choose the C01 and PE tests to reduce misrepresentation of our results due to the number of series to be tested, the length of our time series, and the difficulty in calculating specific parameters, including time embedding parameters necessary for convergence of the more classical methods such as Lyapunov exponents or fractal dimensions. First, our study involves 2028 time series requiring some automation in the methods used. Second, each of our series contains 7001 data points, which is a relatively "short" time series for an unknown system and may not be long enough to represent the full spectrum of the chaotic behavior.[62] To ensure detection of the attractor, a short time series must adhere to a few very specific requirements including having shorter length scales, a folding mechanism inherent inside the attractor, and no noise that is of sufficient length to interfere with the calculations.[62] Since there is no guarantee that the chaotic attractor within fire behavior will possess these features, we would not be able to trust any results from the more classic methods with these shorter time series. Finally, the techniques used in calculating Lyapunov exponents and some fractal dimensions require determining embedding parameters that form the basis for phase-space reconstruction of the dynamical system as described above. By reducing the number of chosen parameters for this study, we reduce the possibility of misrepresentation in our results. In light of these challenges, we choose to use the C01 and PE tests for this study.

A. The 0-1 test

The chaos 0-1 test (C01) has been successfully applied to experimental data, demonstrating its robustness in identifying chaotic phenomena in different real-world settings.[69–72] C01 analyzes the asymptotic growth rate between time steps in a given series.[59,73,74]

1. Description of the steps in the test

The test involves four steps to calculate the asymptotic growth rate between values through time. The advantage of the C01 test lies within the single value output and the visualizations for each step in the process. To illustrate the usefulness of the method, we use the logistic map[75] with a parameter known to be stable ($\mu = 3.5$), and one known to be chaotic ($\mu = 3.91$). In Fig. 4, the column on the left corresponds to the stable parameter, and the column on the right to the chaotic. Each row represents a step in the process and the graphs clearly depict different behaviors for chaotic or stable systems.

For this description, we have reproduced all equations from Gottwald and Melbourne's 2016 paper.[74] The first step translates each of the time series data points using the sine and cosine functions, similar to using the power spectra. Consider a time series $\phi(s),\quad s = 1, \ldots, n$. Then, we translate for each $c \in \{C_n\}$,

$$p_c(n) = \sum_{s=1}^{n} \phi(s)\cos(sc) \quad q_c(n) = \sum_{s=1}^{n} \phi(s)\sin(sc), \tag{7}$$

where we define $\{C_n\}$,

$$\{C_n\}_{n=1}^{100} \in_R \left[\frac{\pi}{5}, \frac{4\pi}{5}\right], \tag{8}$$

where values are randomly chosen from a uniform distribution and applied to this interval, then sorted from smallest to largest. Figures 4(a) and 4(b) show graphs of the translated data for $\mu = 3.5$ [4(a)] and $\mu = 3.91$ [4(b)]. In Fig. 4(a), the stable behavior is structurally symmetric and organized, where in 4(b) we see the disorganization of the time series caused by the chaos.

The second step in the process is to calculate the mean squared displacement for the p's and q's for each $c \in \{C_n\}$. To avoid undersampling, we define n_{cut} as the closest integer to the total number of time steps divided by 10: $n_{cut} = N//10$ and for each $n \in [1, \ldots, n_{cut}]$, we calculate

$$M_{c_i}(n) = \lim_{N\to\infty} \frac{1}{N} \sum_{s=1}^{N} \left[p_{c_i}(s+n) - p_{c_i}(s)\right]^2 + \left[q_{c_i}(s+n) - q_{c_i}(s)\right]^2. \tag{9}$$

We then normalize the mean squared displacement using the squared mean of the series and an oscillation factor,

$$V_{osc}(c,n) = \left(\frac{1}{N}\sum_{s=1}^{N}\phi(s)\right)^2 \frac{1-\cos(cn)}{1-\cos(c)}, \tag{10}$$

such that

$$D_c(n) = M_c(n) - V_{osc}(c,n). \tag{11}$$

The second row in Fig. 4 shows the mean squared displacement in black and the normalized version in red. Figure 4(c) shows the stable case and Fig. 4(d) the chaotic. Note that if we fit a line to either the black or red lines they will have the same slopes which indicates that this normalization process does not affect the growth rate we seek, with Fig. 4(c) showing a general downward or decreasing trend and Fig. 4(d) showing an increasing trend.

Finally, we calculate the asymptotic growth rate for the normalized mean squared displacement using a correlation method. Assuming we have $\vec{n} = \{1, 2, 3, \ldots, n_{cut}\}$ and $\vec{D}_c = \{D_c(n)\}_{n=1}^{n_{cut}}$, we calculate

$$K_c = corr\left(\vec{n}, \vec{D}_c\right) = \frac{cov(\vec{n}, \vec{D}_c)}{\sqrt{var\left(\vec{n}\right), var\left(\vec{D}_c\right)}}, \tag{12}$$

where we use a typical covariance equation,

$$cov(a,b) = \frac{1}{n_{cut}}\sum_{s=1}^{n_{cut}}(a(s)-\bar{a})(b(s)-\bar{b}) \tag{13}$$

and $var(a) = cov(a,a)$. To avoid possible resonance for various c, we define the K value to be the median value of all calculated K_c, which discounts any outliers in the results.

The third row of graphs in Fig. 4 [Figs. 4(e) and 4(f)] show the calculation of the growth rate. We can see that the growth rate in the stable case is declining which indicates this stability, and the growth rate for the chaotic case is increasing, confirming the presence of chaos. The test translates the data using one hundred randomly generated translation variables between $\pi/5$ and $4\pi/5$ defined above as $\{C_n\}$. We use the median growth rate for each of these transition variables so as to avoid resonance or outliers. The last row in Fig. 4 shows the calculated growth rate for all $c \in \{C_n\}$. We can see in Fig. 4(g) that the calculated growth rate for stable behavior in the logistic map is close to 0 when we discount the outlier. For the chaotic case in Fig. 4(h), all of the values are within [0.95, 1] which

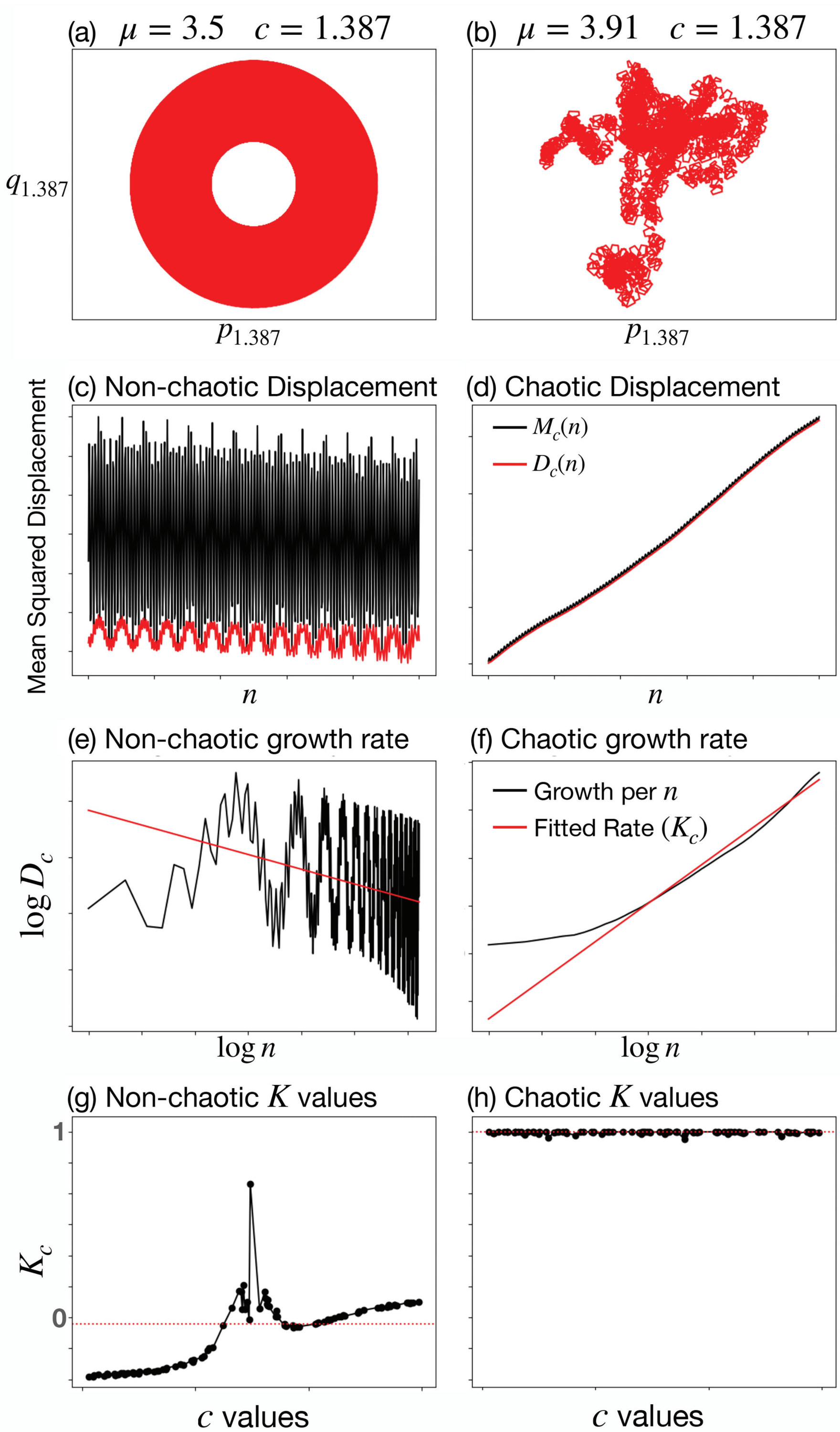

FIG. 4. Visual representation of four steps in the Chaos 0-1 test process applied to the logistic map. Left column relates to a non-chaotic parameter, $\mu = 3.5$, and right column relates to a chaotic parameter, $\mu = 3.91$. The top row is the visual graph of p_c vs q_c. The second row is the mean squared displacement between values for each c and each n, and the third row represents the asymptotic growth rate of the mean squared displacement. The bottom row is the K results for each c and the median value. Note the differences in each visual representation for each step.

indicates chaos as this interval can be defined as "close to 1." In Fig. 4(g), we can see that one of the values is significantly higher than the others. This is most likely due to resonance developed by the specific c value correlating with that jump. Using the median value for the final K_c avoids any interference with these outlier values.

2. Description of the results

The results of the C01 test are represented by the variable K, as defined by the original authors Gottwald and Melbourne.[74] According to their publications,[59,73,74] the test results indicate chaos if the resulting number K is "close to 1" and non-chaotic if K is "close to 0." We seek a more explicit set of values to clearly indicate the results for this test. In Fig. 5, we use the logistic map and plot the K results and the corresponding Lyapunov exponents. We can see that as the Lyapunov exponents increase, the K values also increase to well above the midline of 0.5. As described in Ref. 76, time series that lie on the "edge of chaos," sometimes referred to as "weak" chaos, can be difficult to distinguish as the chaotic signals can be convoluted with noise or a general lack of structure in the series. This style of chaos is represented with very low Lyapunov exponents, like those that are less than 0.19 for μ values below 3.6 in Fig. 5. On the other hand, "high" chaos, as represented in Fig. 5 as Lyapunov exponents above 0.27 ($\mu > 3.65$), are very clearly marked with a C01 test result of $K > 0.9$. As we lack *a priori* knowledge of the noisiness of our series or the general structure of the series in relation to the chaotic signals we are looking for, we choose to include an "inconclusive" range for the results, in which case more examination is needed for official results. We choose the following ranges: the test identifies the system as chaotic ($K \geq 0.5$) or non-chaotic ($K < 0.1$) and we include an "inconclusive range" for $K \in [0.1, 0.5)$. As described in the Gottwald and Melbourne paper from 2008,[77] this does not necessarily infer the absence of chaotic dynamics in the system but that the results require a more in-depth analysis of the steps in the process before concluding the existence of chaos.[77] Since we use the test on 2028 series and, therefore, evaluating each series individually is not feasible for the purposes of this project, we choose the inconclusive range to avoid any false positive results. It should be noted that different choices for these thresholds could affect the results, and this is examined extensively in Sec. IV.

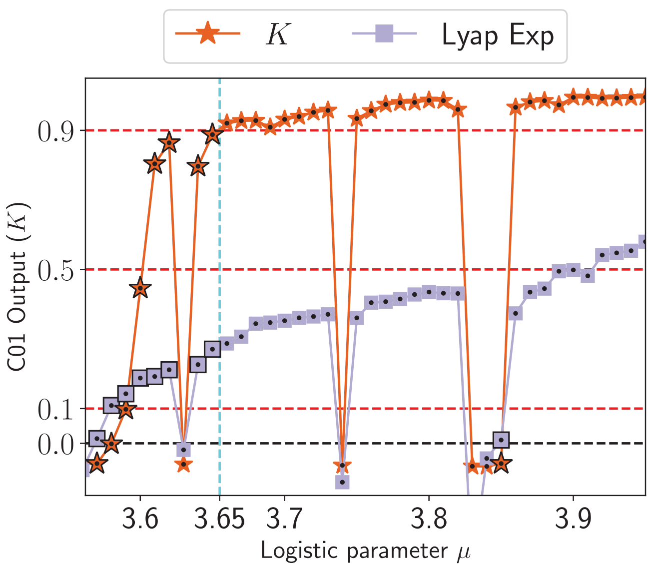

FIG. 5. Output for the C01 test compared with the logistic map Lyapunov exponents. Shows the inconclusive and inaccurate C01 test results for very small Lyapunov exponents indicating very weak chaos. Black outlines indicate positive Lyapunov exponents that correlate to C01 test results below 0.9. Red dotted lines indicate the thresholds for the K conclusions in which $K > 0.5$ indicates chaos, $0.1 \leq K \leq 0.5$ indicates an inconclusive result, and $K < 0.1$ indicates non-chaotic behavior. $K > 0.9$ is presented as a stronger threshold for a positive result. The light blue line at $\mu = 3.6$ shows the threshold for inaccurate C01 test results for weak chaos below this value of μ.

B. Chaotic or stochastic: The PE test

The FIRETEC program is configured to remove all stochastic processes from the simulation and is, therefore, programmatically deterministic. However, the time series creation process may introduce stochasticity through at least two pathways. (i) We are projecting a high-dimensional data onto a univariate time series. Projecting higher-dimensional data into lower dimensions can make it appear noisy due to the "curse of dimensionality," where distances become less meaningful, points crowd the center, and noise can get amplified. (ii) While collecting data, we also vary the length of the time step, and a deterministic signal, if undersampled, can appear stochastic or random because the lack of detail hides its underlying predictable pattern, blurring the deterministic nature into apparent randomness. To accurately capture determinism in a signal, the sampling rate has to be high enough. For example, per the Nyquist–Shannon theorem,[78] to avoid aliasing and preserve signals' predictable nature, the sampling rate must be at least twice the highest frequency. Therefore, we hypothesize that this lack of spatial resolution, along with the time step length, may contribute to stochasticity in our results. The C01 test was designed to identify *deterministic* chaos and may give a false positive result when tested on stochastic time series.[59,74] Thus, we felt it is necessary to test that the design of the series we developed from these data maintains the determinism from the model. We use a Permutation Entropy (PE) test that recognizes stochasticity with two possible outcomes. According to the original developers of the test, the test classifies dynamics as stochastic when $\Omega < 0.1$ or deterministic when $\Omega \geq 0.1$.[60]

Permutation entropy relies on ordinal analysis to find common repeating patterns based on the natural order to a system. For instance, the alphabet has the order a-b-c-d-etc., not p-z-a-r-... or any other combination of letters. Using this "natural order," we can find the likelihood that particular arrangements of letters arise in words by representing these arrangement patterns as a permutation, or a numerical sequence showing their order according to the natural order of the letters. The permutation entropy is then the likelihood of the permutations occurring within the sequence.[79,80]

For instance, consider the series $\{B, D, A, C, E\}$. If we split the series into sequences of length $r = 3$, we have $\{B, D, A\}$, $\{D, A, C\}$, and $\{A, C, E\}$. We then use ordinal analysis to assign a permutation to each sequence based on the order of the letters and which come before or after the others in alphabetical sequence. The list of permutations for $r = 3$ includes $r! = 3! = 6$ possibilities: 123, 231, 312, 213, 321, 132. Consider our first permutation: $\{B, D, A\}$. Since A is the lowest letter in alphabetical order, we assign it a 1. B is the next highest letter, so it becomes 2, and then D is now 3. This makes the permutation, $\{B, D, A\} = 231$. Similarly, we have $\{D, A, C\} = 312$ and $\{A, C, E\} = 123$. We then calculate the permutation entropy of order r for the series as $\sum_{i=1}^{r!} -p_i \log_2(p_i)$, where $r!$ is the total possible permutations of r and p_i = the probability of the ith permutation.[79]

Since our number system also has a natural order, the PE test finds ordinal relations between the values of our time series and calculates the probability of these patterns. When investigating time series with numerical values, we can see that a permutation of 123 indicates that the data are monotonically increasing and 321 indicates monotonically decreasing. Similarly, a permutation of 213 or 312 reveals a local minimum while permutations 132 or 231 reveal a local maximum. Using ordinal analysis with a higher order, like $r = 6$, we can organize the data to find how often the data show a local maximum followed by a local minimum, or other common patterns that could exist. This approach gives a quantity of complexity or irregularity of the system and how it changes between time steps.[80]

The test involves comparing the permutation entropy of a set of stochastic series built from flicker noise to the permutation entropy of our series.[60] Flicker noise is a well known stochastic process where the noise is generated from a power spectrum in which the frequency is inversely proportional to the spectral density.[81] The test calculates the permutation entropy of our time series of order $r = 6$ and, according to Boaretto *et al.*,[60] if the values are similar to those of the flicker noise, (< 0.1 difference) then the time series is designated as stochastic. If the values differ (≥ 0.1), the time series is designated as deterministic. Boaretto *et al.*[60] tested this method on multiple known stochastic and chaotic systems as well as some empirical datasets to show the validity of the method. We illustrate the PE test using 50 normally distributed random series and the logistic map with 50 parameter values (μ) evenly spaced between 3.5 and 4.0, as originally done in Boaretto *et al.*[60] Figure 6 shows that the PE output is close to 0 for the normal random series, strongly indicating stochasticity. The logistic map also accurately presents as deterministic for all runs with $\mu \in [3.5, 4]$ in which the system toggles between deterministic chaos and stability.

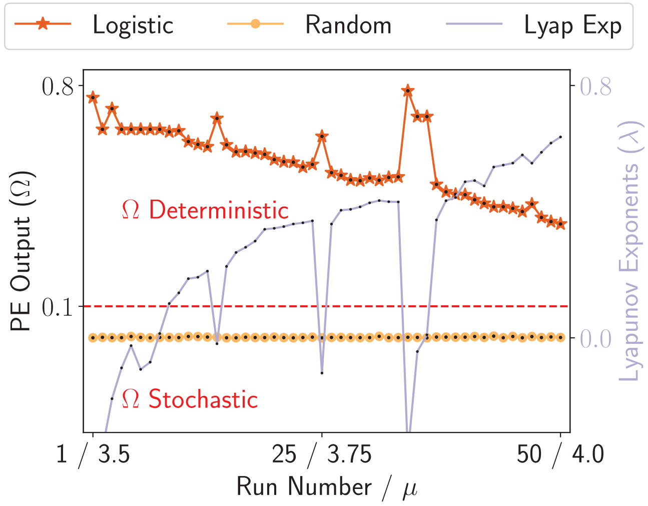

FIG. 6. Output for the Permutation Entropy test used to distinguish between deterministic and stochastic behavior. The logistic results show deterministic behavior for each of 50 runs in which the run number relates to evenly spaced parameter values for $\mu \in [3.5, 4.0]$. The random results show that all 50 normally random series accurately showed stochastic behavior. The Lyapunov exponents presented are calculated from the logistic map for each of the μ values described above. The exponents are a measurement of the rate of divergence between two points that begin very close together. A positive Lyapunov exponent implies divergence, while a negative Lyapunov exponent implies convergence.

IV. RESULTS AND DISCUSSION

In the following figures, we represent all 507 series for each variable $v \in V = \{Q, T, U, w\}$ divided into 39 series at the Fireline, $F_v(x)$, one for each x-coordinate with $x \in X = \{5, 10, 15, \ldots, 195\}$ per variable, v, and 234 for the $I_{v,n}(x)$ and $L_{v,n}(x)$ series, one for each offset coordinate $n \in \{-3, -2, -1, +1, +2, +3\}$ (Sec. II B).

Figure 7 summarizes the results for all 2028 time series and shows how each result for the tests is distributed among the variables. We see that the majority of the series are chaotic with 61.2% of the C01 test results showing chaos. The PE test results are highly deterministic with 98% of the series showing determinism. The highest variance in results from the C01 test occurs in T, while the stochasticity from the PE test results is only showing in the vertical wind velocity, w. Q exhibits deterministic chaos more often than the other three variables. In the following subsections, we dive into these results and hypothesize about the motivating factors for some of these outcomes.

A. Determinism and stochasticity

If a series is deterministic, we can construct a "deterministic map" that inputs a unique value at a particular time step, applies the map, and outputs a corresponding unique value for the next time step with reasonable accuracy. We can see from the bar charts in Fig. 7 that according to the results from the PE test, the fire-induced variables T and Q are entirely deterministic, along with the horizontal wind magnitude, U. The vertical wind velocity, w, however, shows approximately 8% of the runs as stochastic, showing a PE test result of $\Omega < 0.1$. From previous work on wind dynamics done by Lorenz,[15] we know the winds are chaotic in the real world. We hypothesize that the length of the time step, the dimensional reduction, and the spatial resolution for the FIRETEC model contributes to the stochasticity in our results, as discussed in Sec. III B.

To evaluate this hypothesis, we test the sensitivity of our tests to the length of the time step. Unfortunately, due to the extreme computational expense of creating the simulations using FIRETEC, we are restricted from increasing the sampling frequency in our simulation, so we do a minor sensitivity test by decreasing our sampling rate and analyzing the effect on the results of this test. To do this, we test a time series built from every other time step for each x-coordinate in F_v, doubling the length of the time step, from 0.1 s

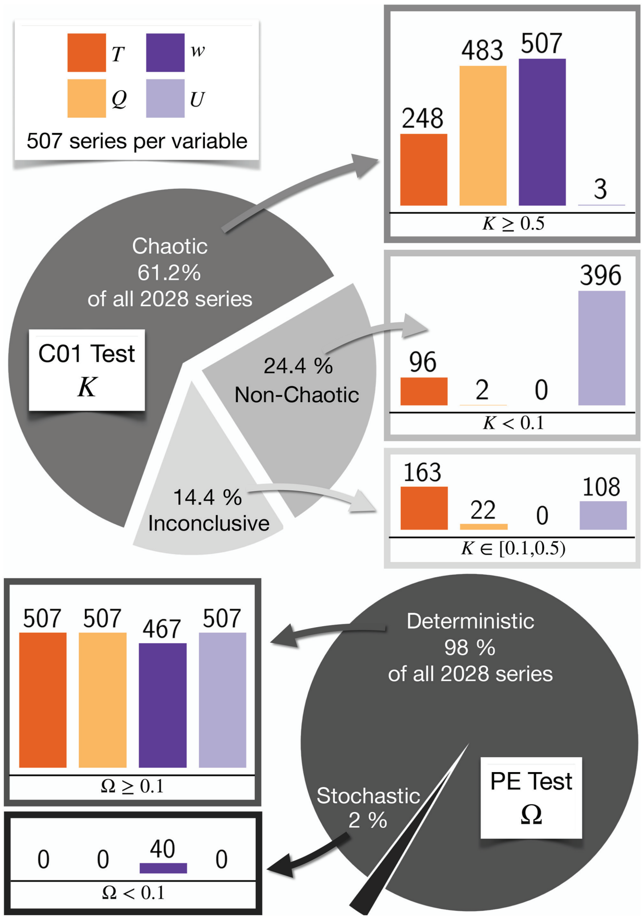

FIG. 7. Pie charts showing results for all 2028 time series per test. The top pie shows the results of the C01 test (K), and the distribution of the results by variable in the corresponding bar charts for each result. The bottom pie shows Ω values from the PE test and their distribution across the variables. Bar charts show how many series of the 507 developed per variable that had the corresponding result.

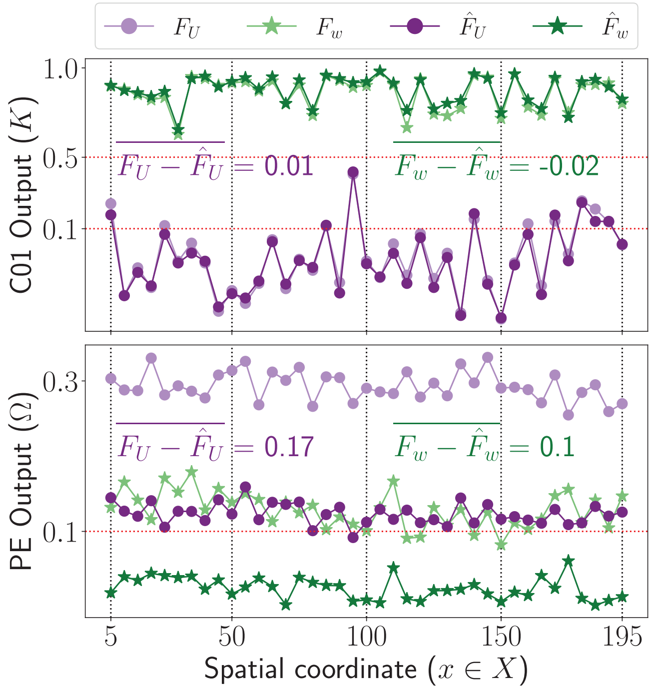

FIG. 8. Results for F_w and F_U with the regular time series and another in which only every other time step was used ($\hat{F}_U$ and $\hat{F}_w$). Note that the C01 test does not show sensitivity to the length of the series whereas both shorter time series for these variables show significantly more stochasticity than the longer series.

to 0.2. These series, $\hat{F}_v$, have only 3500 time steps instead of the original 7001. We find that the C01 test results are very similar for the short and longer series as can be seen in the top panel of Fig. 8 with a mean difference in values on the order of 10^{-2}. The PE test results, however, are significantly lower than with the longer series with a mean difference in values on the order of 10^{-1} (Fig. 8, bottom panel), indicating a sensitivity to the length of the time step for this stochasticity test. While this would be beyond the scope of the present work, future studies should verify this finding by examining the parameter space, including time step length.

B. Variable and spatial analysis

We note that the spatial resolution for these simulations is 2 m $\times$ 2 m per cell, which can be considered large for some of the subgrid turbulent structures in the flow field. When we choose a single value to represent the wind behavior for the entire cell we may be losing information critical to the wind dynamics. In addition to that, we are using the infinite fireline described in Linn *et al.*.[57] According to Canfield *et al.*,[58] changes that could result from this "infinite" fireline include pushing the winds through the fireline rather than being redirected around it, as happens with shorter firelines. Thus, the structure of our infinite fireline may be contributing to the lack of chaos showing in U and the increased stochasticity in w.

We design these series based on the leading edge of the fireline, the point at which combustion initially occurs in the fuel. As can be seen in Fig. 9, all of the F_U series (the horizontal winds) are non-chaotic or inconclusive and the other three variables are clustered with F_Q (convective heat transfer) showing all deterministic chaos and the most clustered values for all series. F_w (vertical wind velocity) is also all chaotic from the C01 test, but four series show stochastic behavior with Ω slightly less than the threshold for the test, 0.1. F_T (temperature) shows a high level of determinism from the PE test, but 5 of the 39 series have an inconclusive C01 test.

There is a strong spatial similarity between the outputs for both tests involving the two fire variable series, F_T and F_Q (Fig. 9), showing the relationship between the temperature of the solid, T, and the temperature's inclination to travel through the gases from one solid fuel to a neighboring cell. We observe high correlations in the outcomes with a Pearson correlation coefficient of 0.742 for our C01 results and 0.811 for the PE results. This means when we see

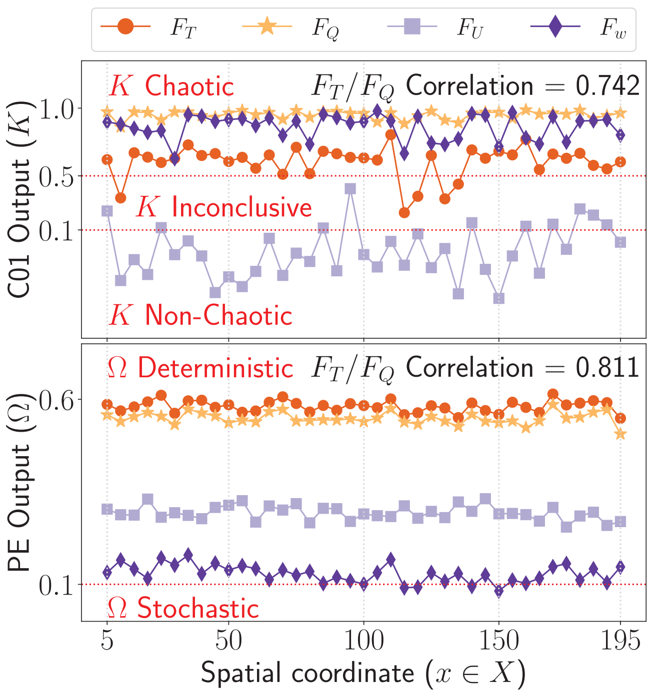

FIG. 9. Results per variable for $F_v(x)$ for all variables $v \in V = \{T, Q, U, w\}$ and all 39 spatial coordinates $x \in X = \{5, 10, 15, \ldots 195\}$. Top panel represents the C01 output (K) and bottom panel shows PE output (Ω).

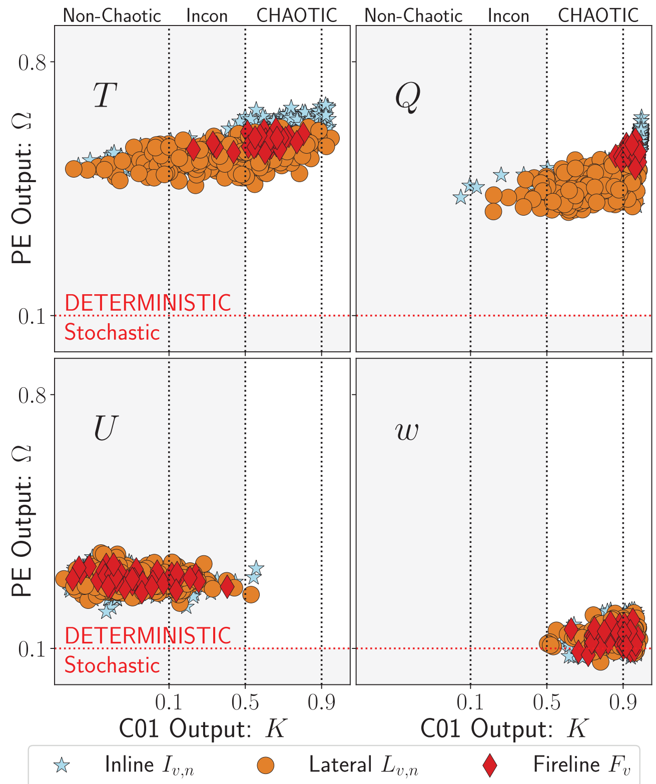

FIG. 10. Plot showing the results for each variable. Red dotted lines delineate the two output results for the PE test (Ω) with deterministic when $\Omega \geq 0.1$ and stochastic when $\Omega < 0.1$. Black dotted lines delineate the three output results for the C01 test (K) with non-chaotic when $K < 0.1$, inconclusive when $K \in [0.1, 0.5)$, and chaotic when $K \geq 0.5$. Each variable set contains 975 total series.

a local maximum or minimum in F_Q there is often a corresponding local maximum or minimum in F_T (Fig. 9). The magnitude of these spikes in the C01 result values (K) is much larger in F_T, but the changes in values between neighboring spatial coordinates have similarities. Since the F_Q values are all close to 1, which is the maximum boundary result for this test, we hypothesize that the magnitude of changes between spatial coordinates are suppressed when the values approach that maximum. In the lower panel of Fig. 9, we can see similar local maximum and minimum correspondence for these two variables as well in the PE (Ω) output. For this determinism result, the magnitudes of the changes are more closely related, presumably because neither set of results is approaching a boundary for the test.

The results are separated by variable and colored by series type in Fig. 10 where we observe a cluster in the bottom right corner of each panel corresponding to Q and w. For T, Q, and U, this cluster is limited to the lateral series results ($L_{v,n}$) and shows a higher C01 test result (stronger chaotic signals) and a lower PE test result (more stochasticity). The lateral series use spatial locations directly perpendicular to the movement of the fireline for the x-coordinate of $F_v(x)$. Because of this construction, these cells may be within the combustion zone at times and in the preheating zone at other times during the course of the series, depending on the structure of the front wave. This means these series are experiencing phase changes within the series, possibly resulting in more chaotic signals. The lateral series ($L_{v,n}$) are also showing more stochasticity than the inline series ($I_{v,n}$), which could also be explained by the phase changes occurring. However, only in w does the PE signal reduce enough to show a clear stochastic result. The w variable is also the most tightly clustered at the bottom right of the graph with all series types very close together, showing that those series were 100% chaotic according to the C01 test with only 61.5% of them being deterministic. As we discuss in Sec. IV A, it is reasonable to assume that many of these stochastic signals would show as deterministic if we were to shorten the length of the time step.

The four variables we investigate for this project are not entirely independent. The behavior of Q is heavily dependent on the wind variables U and w as well as the temperature of the gas and the temperature of the solid, T. Similarly, T is directly affected by the convective heat transfer Q from the surrounding air (see Appendix A 3). Although we separate these components to develop the time series for testing, we must also investigate the results of all four variables together for each type of series. We examine 507 sets of series, each set consisting of all four variables for each series type and location. Even though we have 59.2% of all separate series that are both deterministic and chaotic, we find that none of the time series had all four variables simultaneously exhibit determinism and chaos with U failing 99% of the time. Discounting U, the other three variables show deterministic chaos 43% of the time with T failing most often.

The Inline series ($I_{v,n}$) shows the most variance in the C01 test results spanning all three possible outcomes almost equally in T, and with Q showing mostly chaos with a few inconclusive and non-chaotic results, and U showing mostly non-chaotic results (Fig. 10). To investigate this further, we split the Inline series into those from in front of the fireline in the preheating zone ($1 \leq n \leq 3$) and those behind it ($-3 \leq n \leq -1$) within the combustion zone. Figure 11 shows that for both fire behavior variables T and Q, the series from within the combustion zone are showing far more chaos than those in front of the fireline. Since temperature in front of a fire can jump as much as 1000 K in just a few meters,[82] we see that in the preheating zone, the temperature series are less chaotic as they rise to the ignition temperatures. Once ignition occurs and combustion processes ensue, the chaotic signals increase as expected. This discrepancy does not occur with the U horizontal wind magnitudes, however, which we assume is due to the entrainment processes drawing the winds through the combustion zone from in front and behind the fireline. Since the vertical winds are intricately involved in the three-dimensional flow field and turbulence in the atmosphere, we hypothesize that as the combustion zone approaches the spatial locations in front of the fireline, Wildland Fire Entrainment (WFE) induced flow fields emerge and the ambient winds align with these entrained flows that are drawn into the fireline due to buoyant forces.[83,84] This action appears to organize the horizontal wind magnitude as there is no stochasticity or chaotic signals for U in this region, but it also appears to induce stochasticity in the vertical wind velocity, w. WFE is an established phenomenon that is known to impact combustion zone ventilation and, thus, flame characteristics as well as fire spread and the behavior of merging fire lines,[58,84] and this is a reasonable hypothesis for the organization and lack of chaotic signals present in this region.

From the work of Drossel and Schwabl,[85] Ricotta *et al.*,[41] and Turcotte *et al.*,[39] we know that fire tends toward certain organizational patterns. In fire dynamics, this includes fire whirls[12] and the development of counter-rotational vortices which lead to towers and troughs, a specific phenomenon that can be seen when viewing fire behavior in these marginal conditions.[86] The high level of correlation between F_v and the I_v series indicates that there is a relationship between the fireline and those corresponding coordinates in front and behind the line, which could be indicative of this self-organizing behavior. It is plausible that since we are using univariate time series, the variance in behavior is showing these towers and troughs inside the fireline. We postulate that if we could track the towers and troughs as the fire moves through the domain, we could begin to see how each of these series is affected by their position within this phenomenon. In particular, our work recognizes some spatial commonalities in the series among the fire-induced variables T and Q. These commonalities may indicate new organizing dynamics that will need to be investigated further.

C. Threshold analysis

As stated in Sec. III A, the threshold we choose for our test results could drastically change the results we obtain. Looking at

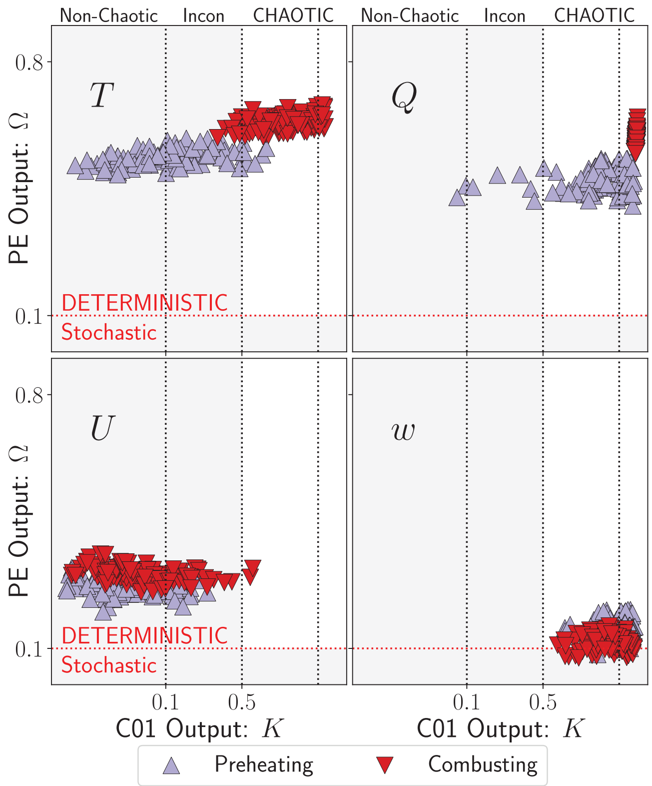

FIG. 11. Results for the Inline series, $I_{v,n}$, colored by spatial location with triangles pointing upwards indicating series in front of the fireline and triangles pointing downward indicating series behind the fireline within the combustion zone.

Fig. 10, we have a vertical line at $K = 0.9$ in addition to the threshold we chose ($K = 0.5$). Examining this figure, we can see that if we move the threshold for chaos detection to 0.9, we vastly increase our inconclusive zone. In fact, our results would change to show only 24% positive for chaotic signals increasing our inconclusive results to 51.6%. This would affect the results for T and Q the most, each losing almost half of their series. The chaotic signals in T fall from 49% chaotic with the lower threshold of 0.5 down to 3% at 0.9, and in Q from 95% down to 46%. From Fig. 11, we see that all of the convective heat transfer series from inside the combustion zone maintain their chaotic signals, so the inconclusive range moves to the preheating zone in front of the fireline. We can also see that all of the remaining T series are also within the combustion zone. As discussed in Sec. III A, the inconclusive range does not indicate stable behavior, but requires a more in-depth analysis of the series to see if there are chaotic signals or not. Given that we see in Fig. 5 that the C01 test struggles with signals "on the edge of chaos," which is also discussed in Gottwald and Melbourne's comment.[77]

Figure 12 shows the changes in results for each variable across five threshold values, $\{0.5, 0.6, 0.7, 0.8, 0.9\}$. The U values were already very low and, therefore, are the least affected by the thresholds. The w output values fall significantly after lowering the threshold to 0.7, losing almost half of the chaotic signals.

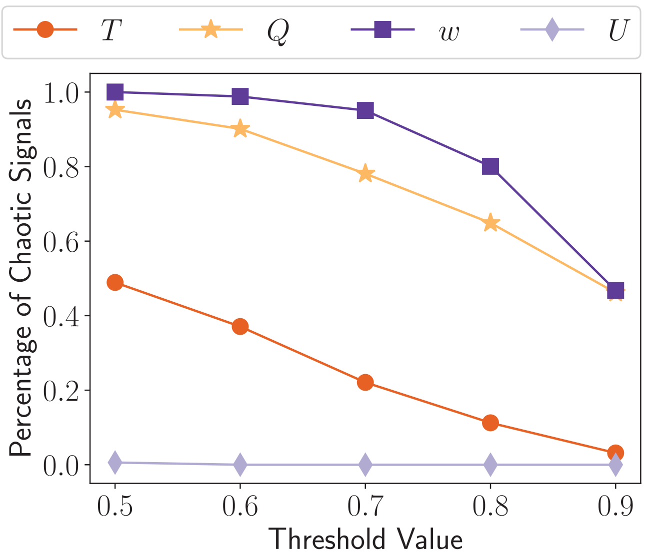

FIG. 12. Changes in results for different threshold values of the C01 test. We test values in {0.5, 0.6, 0.7, 0.8, 0.9}.

Both the convective heat transfer Q and the temperature of the solid, T, lose similar percentages with each threshold lowering, which shows the relationship between these variables clearly.

D. Limitations

We note that there are a few limitations to this study that affect the results. First, we limit our study to a single FIRETEC simulation, using specific fuel and wind parameters that would keep the fire burning but also present marginal fire behavior. By designing our simulation to have cyclic boundary conditions on the lateral sides and designing the time series to be single dimensional, we were able to study several thousand time series from this one simulation. Using a single simulation offers us the ability to analyze the time series without having to factor in simulation parameters as possible causes for the differences in results for each series. Future work should explore the impact of changing simulation parameters that were held constant, such as fuel heterogeneity, moisture levels, time step lengths, and ignition parameters.

We also limit our study to the four variables we consider to be the most influential in fire behavior. As stated in the introduction, the three main drivers for fire behavior include weather, fuel, and topography. We eliminated topography from the simulation and the fuel is homogenous so all the time series would be held constant with those two drivers. For weather, the two wind variables—horizontal wind trajectories (U) and the vertical wind speed (w)—are the main contributors to the flow field when affected by the heat of the fire. The heat variables we choose—the convective heat transfer (Q) and the temperature of the solid (T)—are descriptive of the thermal properties of the fire. Other variables should be considered in future simulations for comparison to the results that are outlined above.

The methodological choices underlying this study warrant careful scrutiny and transparent reflection. Although Sec. III provides a detailed justification for these selections, it is acknowledged that multiple alternative techniques are available for detecting and characterizing chaotic dynamics. A data analysis pipeline was constructed to implement several such methods, including recurrence plots and the computation of various fractal dimension measures, such as the correlation dimension. These methods, however, did not produce robust or reproducible results for the current dataset. This limitation is primarily due to the challenges associated with reliably estimating the necessary embedding parameters. Consequently, these approaches were excluded from the final analysis. Certain nonlinear time series methods circumvent the need for embedding parameter estimation entirely. For example, the approach proposed by Solé and Bascompte[87] enables the estimation of Lyapunov exponents without phase-space reconstruction, making it a promising candidate for future application. The results presented in this study are intended to provide an empirical foundation for more advanced implementations of such techniques. Specifically, the insights gained here may inform more principled parameter selection strategies, motivate the collection of longer observational records, or suggest alternative preprocessing approaches that improve the reliability and interpretability of correlation-dimension and recurrence-based analyses. More broadly, a wide range of analytical tools from complex systems theory remains to be systematically explored in this context. To the authors' knowledge, this work represents an initial and necessary step toward examining fire behavior through the conceptual and mathematical framework of nonlinear dynamics. The findings reported here are expected to stimulate further investigations that will validate, extend, and refine these results using complementary and increasingly sophisticated methodological approaches.

The C01 test suffers from a few limitations that have been highlighted in the literature and should also be acknowledged here. As shown in Fig. 5 and discussed in Secs. III A 2 and IV C, the method can misclassify "weakly" chaotic or intermittently chaotic regimes, where the growth of the mean-squared displacement could be sublinear and the computed K lies in the inconclusive range, making the decision threshold ambiguous.[88] Second, the test is sensitive to additive measurement noise and stochastic perturbations can inflate the mean-squared displacement, producing spurious "chaotic" readings or, conversely, masking true chaos.[74,76] Finally, the 0-1 test does not distinguish among different types of chaotic behavior (e.g., hyperbolic vs non-hyperbolic) and the test's false-positive and false-negative rates increase for high-dimensional systems or heavy turbulence.[74,76,88] While we tried to mitigate these limitations by combining the C01 test with the PE test and examining changes in threshold and results from the logistic map, these limitations may have affected the results we obtained from this study.

It is also important to recognize that the selection of parameters and steps involved in time series construction in the above analyses warrants further scrutiny. Most techniques in nonlinear time-series analysis require several methodological choices, including embedding parameters, thresholds, window lengths, and preprocessing steps; the methods employed in this study are no exception. Although we have provided justification for our parameter selections in the preceding sections, it should be acknowledged that alternative choices could affect the resulting diagnostics. For instance, in Sec. IV C, we demonstrate that the outcomes of the C01 test can vary depending on the selected threshold. Such sensitivity may also depend on how the time series are constructed. In particular, the spatial placement of the measurement series or the choice of reference signals—such as comparisons between interior measurements and those taken near the fireline—could lead to qualitatively different outcomes in the analysis.

The final limitation of this study is our use of a fire simulation without comparison to field collected data. Producing data from field experiments is challenging due to thermal sensitivity for sensor technology, changes in expected environmental conditions during the burn, and due to the chaotic nature of the natural wind field, difficulty matching a FIRETEC simulation to known conditions. We are working on developing an experimental design that minimizes the impact of quantification through measurement on the outcome of the fire behavior, which can be challenging in such a complex system.

V. CONCLUSIONS

A broad range of behaviors has been observed in marginal fires. Some experience sudden extinction, while others transition into self-sustaining fire. In the past, this sensitivity has been studied with respect to initial wind conditions[2,38] and moisture content.[89] We attempt to capture this potential transition point to test the system for the emergence of chaotic dynamics using simulations with FIRETEC, a coupled hydrodynamic-fire behavior model.

FIRETEC Produces Deterministic Chaotic Signals in Fire Behavior. We find the model presents a broad range of results with 61.2% of all 2028 series designated as deterministically chaotic—a result indicating that FIRETEC simulates fire behavior with strong chaotic tendencies. Our study shows that the series tested from the temperature of the solid fuel (T), the convective heat transfer (Q), and the horizontal and vertical wind magnitudes (U and w) all produce chaotic signals in different circumstances, depending on spatial location, time series design, and characteristics of the variables under review. The preheating zone in front of the fireline shows far less chaos than from within the combustion zone, a result that supports the original conjecture that ignition causes a phase change in the behavior of these variables.

Stochasticity Comes From Model and Analysis Design. We find stochasticity from the Permutation Entropy (PE) test in our vertical wind velocity time series. We also find that the PE test is sensitive to the length of the time step and longer time steps produce more stochastic results. The structure of the domain may also contribute to the stochasticity in our results as a spatial resolution of 2 m $\times$2 m may be too large to detect the sub-grid turbulent structures of the flow field. The infinite fireline in the design of our simulation may also be interrupting the natural entrainment processes, as well as the dimensional reduction necessary for our methods of detecting chaotic signals.

Spatial Relationships Affect Chaotic Signals. The preheating zone in front of the fireline shows less chaotic behaviors as the temperatures rise to ignition, and the combustion zone shows more chaotic signals, as expected. The infinite fireline we use in the design for our simulation may directly contribute to the structure of the flow field, affecting the horizontal wind magnitudes (U) more than the other variables in the study. We also find that our fire-induced variables, T and Q, are highly correlated when compared for the same spatial coordinate series.

ACKNOWLEDGMENTS

This research was supported by the Los Alamos National Laboratory (LANL) through its Center for Space and Earth Science (CSES). CSES is funded by LANL's Laboratory Directed Research and Development (LDRD) program under Project No. 20180475DR. Additional funding was provided by the Center for Non-Linear Studies through LDRD at LANL. This research used resources provided by the Los Alamos National Laboratory Institutional Computing Program, which is supported by the U.S. Department of Energy National Nuclear Security Administration under Contract No. 89233218CNA000001.

AUTHOR DECLARATIONS

Conflict of Interest

The authors have no conflicts to disclose.

Author Contributions

Jenna Sjunneson McDanold: Formal analysis (equal); Funding acquisition (supporting); Methodology (equal); Software (lead); Visualization (lead); Writing – original draft (lead); Writing – review & editing (lead). **Alex Jonko:** Conceptualization (equal); Formal analysis (equal); Funding acquisition (lead); Methodology (equal); Writing – review & editing (supporting). **Kara Yedinak:** Conceptualization (equal); Formal analysis (equal); Funding acquisition (supporting); Methodology (equal); Writing – review & editing (supporting). **Rod Linn:** Conceptualization (equal); Formal analysis (equal); Methodology (equal); Writing – review & editing (supporting). **Sophie Bonner:** Resources (equal); Writing – review & editing (supporting). **Alexander Josephson:** Resources (equal); Writing – review & editing (supporting). **Nishant Malik:** Formal analysis (equal); Methodology (equal); Supervision (lead); Writing – review & editing (supporting).

DATA AVAILABILITY

The data that support the findings of this study are available from the corresponding author upon reasonable request.

APPENDIX A: HIGRAD-FIRETEC

Here we describe the governing equations for calculating the variables we used within FIRETEC and its coupled hydrodynamic solver HIGRAD. HIGRAD-FIRETEC is, in its essence, a modified Navier–Stokes system that takes an ignition sequence and a fuel bed or canopy arrangement as inputs. FIRETEC works with HIGRAD to track the fire movement throughout the domain space. HIGRAD is an atmospheric simulator that uses a Method of Averages scheme to decrease computational expense.[82]

1. Definitions

- **Solid**: The combination of the combustible fuel and the water within a given material.
- **Fuel**: The dry portion of the solid.
- **Cell**: The three-dimensional cube at a given coordinate in the FIRETEC domain space.
- **Cylinder**: The basic building blocks of the fuel within a particular FIRETEC cell; all fuel is modeled to be made up of several cylinders such that environmental factors may move through the area in between each cylinder.

2. *Q*

Q stands for Convective Heat Transfer and is used in FIRETEC to describe the transfer of heat from the gas to the solid within a given cell. It is positive when the gas in the cell is hotter than the solid in the cell as it is measured from the perspective of the solid. The equation is related to the basic convective heat transfer formula from Çengel and Ghajar,[90]

$$Q = h\gamma(T_g - T), \tag{A1}$$

where

- h is the convective heat transfer coefficient (units = W m^{-2} K^{-1}),
- γ is a scaling coefficient based on the relationship of the bulk density to the true density,
- T_g is the temperature of the gas in the cell, and
- T is the temperature of the solid.

Note that since we are subtracting T from T_g, this value can be negative when the gas in the cell is cooler than the solid. We define each of these parameters below.

The parameter h can be derived from using the Nusselt number, which in thermodynamics can be defined as the ratio of the convective heat transfer to the conductive heat transfer,

$$Nu = \frac{h}{C_p/L} = \frac{hL}{C_p}, \tag{A2}$$

where C_p is the thermal conductivity or specific heat of the air (units = W m^{-1} K^{-1}), and L is a characteristic length which we define as the radius of the cylinder (units = m). When we solve for h in this equation, we find

$$h = \frac{NuC_p}{L}. \tag{A3}$$

In practice, we define the Nusselt number as a function of the Reynold's number to represent forced convection within the fire. In FIRETEC, the vegetation is modeled as a collection of cylinders of ranging sizes (i.e., 0.005 m for grass) so that the wind may travel through the cylinders and spread the fire. Thus, we use a Nusselt number associated with crossflow wind across a cylinder,[91]

$$Nu = 0.683Re^{0.466}, \tag{A4}$$

and altogether we get

$$h = 0.683Re^{0.466}\frac{C_p}{L}, \tag{A5}$$

with units of W/m^{-2} K^{-1}.

For the parameter γ, we use an area per volume and define it as the ratio of the bulk density of the fuel in the cylinder to the true density of the fuel, multiplied by the radius of the cylinder, L. The bulk density of the fuel ρ_f is defined as the mass of the fuel to the volume of the cell, and the true density of the fuel ρ_0 is defined as the mass of the fuel to the volume of the fuel,

$$\gamma = 2a\frac{\rho_f}{\rho_0}\frac{1}{L}, \tag{A6}$$

where a is a dimensionless correction factor for a change in the orientation of the cylinder. This equation can be expressed as being the surface area of the cylinder to the volume of the cell and has units $1/m$.

3. *T*

T stands for the temperature of the solid. Using conservation of energy laws, this quantity is calculated using the specific internal energy of the solid (E_s) divided by the heat capacity for the solid material at a constant pressure ($C_{p,s}$),

$$T = \frac{E_s}{C_{p,s}}. \tag{A7}$$

We use the Kopp–Neumann Law[92] to define $C_{p,s}$,

$$C_{p,s} = \frac{\rho_w C_{p,w} + \rho_F C_{p,f}}{\rho_w + \rho_f}, \tag{A8}$$

where we take the density of the water within the solid, ρ_w, and multiply it by the specific heat of the water at constant pressure, $C_{p,w}$. We add that to ρ_F, the density of the fuel within the solid, multiplied by the specific heat of the fuel at constant pressure, $C_{p,f}$; and divide that sum by $\rho_w + \rho_f = \rho_s$, the total density of the solid. We define the change in the energy of the solid (E_S) as

$$\frac{dE_s}{dt} = Q_{conv} + \theta_s \Delta H_{RXN} - E_{f,m} + \Delta H_{EVAP} - E_{w,m} + R_s, \tag{A9}$$

where we have

- Q = the convective heat transfer (see Appendix A 2)
- $\theta_S \Delta H_{RXN}$ = the amount of energy from combustion returning to the solid with
  - θ_S = the proportion of the combustion energy that returns to the solid and
  - ΔH_{RXN} = the total energy generated through the combustion reaction
- $E_{f,m} = m_f C_{p,f} T_{RXN}$ is the loss of energy attributed to mass loss during combustion with
  - m_f = mass of fuel lost
  - $C_{p,f}$ = heat capacity of the fuel
  - T_{RXN} = temperature of the combustion reaction
- ΔH_{EVAP} = amount of energy lost due to evaporation of the water in the solid
- $E_{w,m}$ = the loss of energy attributed to water loss through evaporation
- $R_s = -0.8\sigma\gamma(T^4 - T_A^4)$ is the energy added to the solid through radiation with
  - -0.8 is an emissivity constant for the fuel

– $\sigma = 5.678e - 8$ is the Stefan–Boltzmann constant
– γ is defined as in Eq. (A6)
– $T =$ the temperature of the solid, and
– $T_A =$ the ambient temperature.

4. Wind variables

The horizontal wind magnitude we are using, $UV = \sqrt{u^2 + v^2}$ and the vertical wind velocity W are calculated using HIGRAD, the hydrodynamics solver coupled with FIRETEC. A complete description and all equations associated with these variables can be found in Reisner *et al.*[82]

REFERENCES

[1]C. B. Clements, N. P. Lareau, D. Seto, J. Contezac, B. Davis, C. Teske, T. J. Zajkowski, A. T. Hudak, B. C. Bright, M. B. Dickinson, B. W. Butler, D. Jimenez, and J. K. Hiers, "Fire weather conditions and fire–atmosphere interactions observed during low-intensity prescribed fires—RxCADRE 2012," Int. J. Wildland Fire **25**, 90–101 (2016).
[2]A. K. Jonko, K. M. Yedinak, J. L. Conley, and R. R. Linn, "Sensitivity of grass fires burning in marginal conditions to atmospheric turbulence," J. Geophys. Res.: Atmos. **126**, e2020JD033384 (2021).
[3]J. G. Quintiere, *Principles of Fire Behavior* (Delmar Publishers, 1998).
[4]J. M. Iniguez, T. W. Swetnam, and S. R. Yool, "Topography affected landscape fire history patterns in southern Arizona, USA," For. Ecol. Manage. **256**, 295–303 (2008).
[5]C. B. Clements and D. Seto, "Observations of fire–atmosphere interactions and near-surface heat transport on a slope," Boundary-Layer Meteorol. **154**, 409–426 (2015).
[6]C. Airey-Lauvaux, A. D. Pierce, C. N. Skinner, and A. H. Taylor, "Changes in fire behavior caused by fire exclusion and fuel build-up vary with topography in California montane forests, USA," J. Environ. Manage. **304**, 114255 (2022).
[7]B. M. Kilgore and R. W. Sando, "Crown-fire potential in a sequoia forest after prescribed burning," For. Sci. **21**, 83–87 (1975).
[8]K. M. Menning and S. L. Stephens, "Fire climbing in the forest: A semiqualitative, semiquantitative approach to assessing ladder fuel hazards," Western J. Appl. For. **22**, 88–93 (2007).
[9]A. Alvarez, M. Gracia, and J. Retana, "Fuel types and crown fire potential in pinus halepensis forests," Eur. J. For. Res. **131**, 463–474 (2012).
[10]B. E. Potter, "Atmospheric interactions with wildland fire behaviour—I. Basic surface interactions, vertical profiles and synoptic structures," Int. J. Wildland Fire **21**, 779–801 (2012).
[11]B. E. Potter, "Atmospheric interactions with wildland fire behaviour—II. Plume and vortex dynamics," Int. J. Wildland Fire **21**, 802–817 (2012).
[12]N. P. Lareau, N. J. Nauslar, E. Bentley, M. Roberts, S. Emmerson, B. Brong, M. Mehle, and J. Wallman, "Fire-generated tornadic vortices," Bull. Am. Meteorol. Soc. **103**, E1296–E1320 (2022).
[13]W. Mell, M. A. Jenkins, J. Gould, and P. Cheney, "A physics-based approach to modelling grassland fires," Int. J. Wildland Fire **16**, 1–22 (2007).
[14]R. Linn, J. Reisner, J. J. Colman, and J. Winterkamp, "Studying wildfire behavior using FIRETEC," Int. J. Wildland Fire **11**, 233–246 (2002).
[15]E. N. Lorenz, "Deterministic nonperiodic flow," J. Atmos. Sci. **20**, 130–141 (1963).
[16]J. Banks, J. Brooks, G. Cairns, G. Davis, and P. Stacey, "On Devaney's definition of chaos," Am. Math. Mon. **99**, 332–334 (1992).
[17]R. Brown and L. O. Chua, "Clarifying chaos: Examples and counterexamples," Int. J. Bifurcation Chaos **06**, 219–249 (1996).
[18]B. R. Hunt and E. Ott, "Defining chaos," Chaos **25**, 097618 (2015).
[19]E. Sander and J. A. Yorke, "The many facets of chaos," Int. J. Bifurcation Chaos **25**, 1530011 (2015).
[20]S. H. Strogatz, *Nonlinear Dynamics and Chaos: With Applications to Physics, Biology, Chemistry, and Engineering*, 2nd ed. (CRC Press, Boca Raton, 2019).
[21]A. Mashuri, N. H. Adenan, N. S. Abd Karim, W. T. Siew, and Z. Zeng, "Application of chaos theory in different fields—A literature review," J. Sci. Math. Lett. **12**, 92–101 (2024).
[22]D. Merritt and M. Valluri, "Chaos and mixing in triaxial stellar systems," Astrophys. J. **471**, 82 (1996).
[23]M. Lecar, F. A. Franklin, M. J. Holman, and N. W. Murray, "Chaos in the solar system," Annu. Rev. Astron. Astrophys. **39**, 581–631 (2001).
[24]K. M. Deck, M. J. Holman, E. Agol, J. A. Carter, J. J. Lissauer, D. Ragozzine, and J. N. Winn, "Rapid dynamical chaos in an exoplanetary system," Astrophys. J. **755**, L21 (2012).
[25]B. P. Wilcox, M. S. Seyfried, and T. H. Matison, "Searching for chaotic dynamics in snowmelt runoff," Water Resour. Res. **27**, 1005–1010 (1991).
[26]S. Maus and V. Dimri, "Properties of potential fields," J. Assoc. Expl. Geophys. **16**, 131–139 (1995).
[27]M. R. Prakash and V. P. Dimri, "Distribution of the aftershock sequence of the Latur earthquake in time and space by fractal approach," J. Geol. Soc. India **55**, 167–174 (2000).
[28]K. V. Koshel' and S. V. Prants, "Chaotic advection in the ocean," Phys.-Usp. **49**, 1151 (2006).
[29]S.-A. Ouadfeul, L. Aliouane, and A. Boudella, "Fractal and chaos in exploration geophysics," in *Fractal Analysis and Chaos in Geosciences* (IntechOpen Limited, 2012).
[30]J. E. Skinner, M. Molnar, T. Vybiral, and M. Mitra, "Application of chaos theory to biology and medicine," Integr. Physiol. Behav. Sci. **27**, 39–53 (1992).
[31]M. I. Rabinovich and H. D. I. Abarbanel, "The role of chaos in neural systems," Neuroscience **87**, 5–14 (1998).
[32]K. Warren, C. Franklin, and C. L. Streeter, "New directions in systems theory: Chaos and complexity," Social Work **43**, 357–372 (1998).
[33]X. Lu, D. Clements-Croome, and M. Viljanen, "Integration of chaos theory and mathematical models in building simulation: Part II: Conceptual frameworks," Autom. Constr. Build. **19**, 452–457 (2010).
[34]B. Sivakumar, "Chaos theory in geophysics: Past, present and future," Chaos Solitons Fractals **19**, 441–462 (2004).
[35]G. S. Duane and J. J. Tribbia, "Synchronized chaos in geophysical fluid dynamics," Phys. Rev. Lett. **86**, 4298–4301 (2001).
[36]G. B. Pasternack, "Does the river run wild? Assessing chaos in hydrological systems," Adv. Water Resour. **23**, 253–260 (1999).
[37]W. Marzocchi, F. Mulargia, and G. Gonzato, "Detecting low-dimensional chaos in geophysical time series," J. Geophys. Res.: Solid Earth **102**, 3195–3209 (1997).
[38]R. R. Linn, J. L. Winterkamp, J. H. Furman, B. Williams, J. K. Hiers, A. Jonko, J. J. O'Brien, K. M. Yedinak, and S. Goodrick, "Modeling low intensity fires: Lessons learned from 2012 RxCADRE," Atmosphere **12**, 139 (2021).
[39]D. L. Turcotte, S. G. Abaimov, R. Shcherbakov, and J. B. Rundle, "Nonlinear dynamics of natural hazards," in *Nonlinear Dynamics in Geosciences* (Springer, 2007), pp. 557–580.
[40]P. Bak, C. Tang, and K. Wiesenfeld, "Self-organized criticality: An explanation of the 1/*f* noise," Phys. Rev. Lett. **59**, 381–384 (1987).
[41]C. Ricotta, G. Avena, and M. Marchetti, "The flaming sandpile: Self-organized criticality and wildfires," Ecol. Model. **119**, 73–77 (1999).
[42]J. Mampel Danta, V. N. Egorova, and G. Pagnini, "Predicting the arrival of the unpredictable: An approach for foreseeing the transition to chaos of wildfire propagation," Commun. Nonlinear Sci. Numer. Simul. **138**, 108190 (2024).
[43]H. Kantz and T. Schreiber, *Nonlinear Time Series Analysis*, 2nd ed. (Cambridge University Press, 2003).
[44]N. Malik, "Uncovering transitions in paleoclimate time series and the climate driven demise of an ancient civilization," Chaos **30**, 083108 (2020).
[45]J. R. Curry and W. L. Fons, "Rate of spread of surface fires in the ponderosa pine type of California," J. Agric. Res. **57**, 239–267 (1938).
[46]W. L. Fons, "Analysis of fire spread in light forest fuels," J. Agric. Res. **72**, 93–121 (1946).
[47]P. Bak, K. Chen, and C. Tang, "A forest-fire model and some thoughts on turbulence," Phys. Lett. A **147**, 297–300 (1990).
[48]A. Bakhshaii and E. A. Johnson, "A review of a new generation of wildfire–atmosphere modeling," Can. J. For. Res. **49**, 565–574 (2019).
[49]R. C. Rothermel, "A mathematical model for predicting fire spread in wildland fuels," Research Paper INT-115 (1972), google-Books-ID: AfyMv5NBSjoC.

[50]J. Barber, C. Bose, A. Bourlioux, J. Braun, E. Brunelle, R. Bryce, T. Garcia, T. Hillen, C. Lam, B. Ong, C. Poschl, and C. Tymstra, "PROMETHEUS—Canada's wildfire growth simulator," Technical Report DMS-861-IR, 2007.
[51]R. Linn, J. Winterkamp, J. J. Colman, C. Edminster, and J. D. Bailey, "Modeling interactions between fire and atmosphere in discrete element fuel beds," Int. J. Wildland Fire **14**, 37–48 (2005).
[52]C. M. Hoffman, J. Canfield, R. R. Linn, W. Mell, C. H. Sieg, F. Pimont, and J. Ziegler, "Evaluating crown fire rate of spread predictions from physics-based models," Fire Technol. **52**, 221–237 (2016).
[53]F. Pimont, J.-L. Dupuy, R. R. Linn, and S. Dupont, "Impacts of tree canopy structure on wind flows and fire propagation simulated with FIRETEC," Ann. For. Sci. **68**, 523–530 (2011).
[54]F. Pimont, R. Parsons, E. Rigolot, F. de Coligny, J.-L. Dupuy, P. Dreyfus, and R. R. Linn, "Modeling fuels and fire effects in 3D: Model description and applications," Environ. Model. Softw. **80**, 225–244 (2016).
[55]G. Marshall, D. K. Thompson, K. Anderson, B. Simpson, R. Linn, and D. Schroeder, "The impact of fuel treatments on wildfire behavior in North American boreal fuels: A simulation study using FIRETEC," Fire **3**, 18 (2020).
[56]N. W. C. Group, "8.6 Head, Flank, and Rear Fire Terms | NWCG" (2023). See https://www.nwcg.gov/course/ffm/fire-behavior/firefighter-math-86-head-flank-and-rear-fire-terms
[57]R. R. Linn, J. M. Canfield, P. Cunningham, C. Edminster, J. L. Dupuy, and F. Pimont, "Using periodic line fires to gain a new perspective on multi-dimensional aspects of forward fire spread," Agric. For. Meteorol. **157**, 60–76 (2012).
[58]J. M. Canfield, R. R. Linn, J. A. Sauer, M. Finney, and J. Forthofer, "A numerical investigation of the interplay between fireline length, geometry, and rate of spread," Agric. For. Meteorol. **189-190**, 48–59 (2014).
[59]G. A. Gottwald and I. Melbourne, "A new test for chaos in deterministic systems," Proc. R. Soc. London, Ser. A **460**, 603–611 (2004).
[60]B. R. R. Boaretto, R. C. Budzinski, K. L. Rossi, T. L. Prado, S. R. Lopes, and C. Masoller, "Discriminating chaotic and stochastic time series using permutation entropy and artificial neural networks," Sci. Rep. **11**, 15789 (2021).
[61]P. Grassberger and I. Procaccia, "Estimation of the Kolmogorov entropy from a chaotic signal," Phys. Rev. A **28**, 2591–2593 (1983).
[62]A. Wolf, J. B. Swift, H. L. Swinney, and J. A. Vastano, "Determining Lyapunov exponents from a time series," Phys. D **16**, 285–317 (1985).
[63]J. P. Eckmann, S. O. Kamphorst, D. Ruelle, and S. Ciliberto, "Liapunov exponents from time series," Phys. Rev. A **34**, 4971–4979 (1986).
[64]S. Sato, M. Sano, and Y. Sawada, "Practical methods of measuring the generalized dimension and the largest Lyapunov exponent in high dimensional chaotic systems," Prog. Theor. Phys. **77**, 1–5 (1987).
[65]M. T. Rosenstein, J. J. Collins, and C. J. De Luca, "A practical method for calculating largest Lyapunov exponents from small data sets," Physica D **65**, 117–134 (1993).
[66]C. Touzé and A. Chaigne, Lyapunov exponents from experimental time series: Application to cymbal vibrations," Acta Acust. Acust. **86**, 557–567 (2000). See https://ensta.hal.science/hal-01134813/
[67]G. Akemann, Z. Burda, and M. Kieburg, "From integrable to chaotic systems: Universal local statistics of Lyapunov exponents," Europhys. Lett. **126**, 40001 (2019).
[68]P. Grassberger and I. Procaccia, "Measuring the strangeness of strange attractors," Physica D **9**, 189–208 (1983).
[69]G. Litak, A. Syta, M. Budhraja, and L. M. Saha, "Detection of the chaotic behaviour of a bouncing ball by the 0–1 test," Chaos, Solitons Fractals **42**, 1511–1517 (2009).
[70]G. Litak, A. Syta, and M. Wiercigroch, "Identification of chaos in a cutting process by the 0–1 test," Chaos, Solitons Fractals **40**, 2095–2101 (2009).
[71]M. A. Savi, F. H. I. Pereira-Pinto, F. M. Viola, A. S. de Paula, D. Bernardini, G. Litak, and G. Rega, "Using 0–1 test to diagnose chaos on shape memory alloy dynamical systems," Chaos, Solitons Fractals **103**, 307–324 (2017).
[72]A. Ouannas, A.-A. Khennaoui, S. Momani, and V.-T. Pham, "The discrete fractional duffing system: Chaos, 0–1 test, C complexity, entropy, and control," Chaos **30**, 083131 (2020).
[73]G. A. Gottwald and I. Melbourne, "On the validity of the 0–1 test for chaos," Nonlinearity **22**, 1367–1382 (2009).
[74]G. A. Gottwald and I. Melbourne, *Chaos Detection and Predictability* (Springer, Berlin, 2016), pp. 221–247.
[75]E. D. Lorenz, "The problem of deducing the climate from the governing equations," Tellus A **16**, 1 (2024).
[76]J. Hu, W.-W. Tung, J. Gao, and Y. Cao, "Reliability of the 0-1 test for chaos," Phys. Rev. E **72**, 056207 (2005).
[77]G. A. Gottwald and I. Melbourne, "Comment on "Reliability of the 0-1 test for chaos"," Phys. Rev. E **77**, 028201 (2008).
[78]C. E. Shannon, "Communication in the presence of noise," Proc. IRE **37**, 10–21 (1949).
[79]C. Bandt and B. Pompe, "Permutation entropy: A natural complexity measure for time series," Phys. Rev. Lett. **88**, 174102 (2002).
[80]M. Henry and G. Judge, "Permutation entropy and information recovery in nonlinear dynamic economic time series," Econometrics **7**, 10 (2019).
[81]J. Barnes and D. Allan, "A statistical model of flicker noise," Proc. IEEE **54**, 176–178 (1966).
[82]J. Reisner, S. Wynne, L. Margolin, and R. Linn, "Coupled atmospheric–fire modeling employing the method of averages," Mon. Weather Rev. **128**, 3683–3691 (2000).
[83]E. E. Zukoski, T. Kubota, and B. Cetegen, "Entrainment in fire plumes," Fire Saf. J. **3**, 107–121 (1981).
[84]R. R. Linn, J. K. Hiers, J. J. O'Brien, K. Yedinak, C. Hoffman, J. Canfield, D. Robinson, and S. Goodrick, "Wildland fire entrainment: The missing link between wildland fire and its environment," PNAS Nexus **4**, 576 (2024).
[85]B. Drossel and F. Schwabl, "Self-organized critical forest-fire model," Phys. Rev. Lett. **69**, 1629–1632 (1992).
[86]T. Banerjee, T. Holland, K. Solander, M. Holmes, and R. Linn, "Identifying characteristics of wildfire towers and troughs," Atmosphere **11**, 796 (2020).
[87]R. V. Solé and J. Bascompte, "Measuring chaos from spatial information," J. Theor. Biol. **175**, 139–147 (1995).
[88]D. Bernardini and G. Litak, "An overview of 0–1 test for chaos," J. Braz. Soc. Mech. Sci. Eng. **38**, 1433–1450 (2016).
[89]R. A. Wilson JR., "Observations of extinction and marginal burning states in free burning porous fuel beds," Combust. Sci. Technol. **44**, 179–193 (1985).
[90]Y. Çengel and A. Ghajar, *Heat and Mass Transfer: Fundamentals & Applications* (McGraw-Hill Education, 2019).
[91]E. Edge and E. E. LLC, "Nusselt number for forced convection" (2023). See https://www.engineersedge.com/heat_transfer/nusselt_number_13856.htm
[92]S. K. Kauwe, J. Graser, A. Vazquez, and T. D. Sparks, "Machine learning prediction of heat capacity for solid inorganics," Integr. Mater. Manufac. Innov. **7**, 43–51 (2018).